

Simpler is Faster: Practical Distance Reporting by Sorting Along a Space-Filling Curve*

Sarita de Berg[†] Emil Toftegaard Gæde[‡] Ivor van der Hoog[†] Eva Rotenberg[†]

Abstract. Range reporting is a classical problem in computational geometry. A (rectangular) reporting data structure stores a point set P of n points, such that, given a (rectangular) query region Δ , it returns all points in $P \cap \Delta$. A variety of data structures support such queries with differing asymptotic guarantees:

- k -d trees: $O(\sqrt{n} + |P \cap \Delta|)$ expected time,
- range trees: $O(\log^2 n + |P \cap \Delta|)$ worst-case time,
- R -trees: $O(\log n + |P \cap \Delta|)$ expected time.

Quadtrees support approximate range queries in expected logarithmic time under mild input assumptions.

A common variant of range queries are *distance reporting queries*, where the input is a query point q and a radius δ , and the goal is to report all points in P within distance δ of q . Such queries frequently arise as sub-routines in geometric data structure construction and in Fréchet distance computations. Modern implementations typically reduce distance queries to rectangular range queries using the data structures listed above.

We revisit a simple and practical heuristic for distance reporting, originally proposed by Asano, Ranjan, Roos, and Welzl (TCS '97). The approach is straightforward: sort the input point set P along a space-filling curve. Queries then reduce to scanning at most four contiguous ranges along the sorted curve.

We show extensive experimental evaluation of modern distance and range reporting data structures. In a static scenario, we show that this simple technique is competitive with all but the most highly optimised range reporting data structures. Notably, these involved structures use space-filling curves themselves to speed up computation. In a dynamic setting, our simpler method even becomes the preferred technique.

This leads to a perhaps unexpected insight: while modern data structures invest heavily in leveraging

space-filling curves for optimising their layout and traversal, it is the curve itself, rather than the surrounding machinery, that delivers much of the performance.

Acknowledgements. This work was supported by the Carlsberg Foundation Fellowship CF21-0302 “Graph Algorithms with Geometric Applications”, and the VILLUM Foundation grant (VIL37507) “Efficient Recomputations for Changeful Problems”. Part of this work took place while Ivor van der Hoog and Eva Rotenberg were affiliated with the Technical University of Denmark.

*Our repository is available at: <https://anonymous.4open.science/r/SFC-Index>. We derive our clustering benchmark from: <https://anonymous.4open.science/r/discrete-subtrajectory-clustering>. These repositories will be made publicly available under open access upon acceptance.

[†]IT University of Copenhagen, Denmark

[‡]Technical University of Denmark, Denmark

1 Introduction.

Distance reporting queries consist of a point q and a distance δ . The goal is to output all points of the input P within distance δ of q . This is a classical problem that frequently arises in application domains. In recent years, several implementation papers use a distance reporting data structure as a subroutine [1, 9, 14, 15, 19, 32, 34]. We show a simple technique for efficient and practical distance reporting. We compare our technique to state-of-the-art data structures to show that our approach is not only simpler, but even competitive in a static setting and more efficient dynamically. In full generality, our theoretical results apply to \mathbb{R}^d , but we focus our implementation and experiments on the plane.

1.1 Related theory. Distance reporting queries can be reduced to range reporting queries, and all related work primarily considers range queries. Under the L_1 or L_∞ metric, any rectangle reporting data structure can answer distance queries. Under the L_2 metric, one can either reduce the problem to rectangular distance queries in \mathbb{R}^3 , or, query with a bounding square and filter the results. Whilst the latter technique has no asymptotic performance guarantees, it is the common technique in practice because range queries become inefficient as the dimension increases.

Rectangular range reporting in theory. A wide body of literature exists on data structures for (planar) range reporting. Let k denote the output size of a (rectangular) range query. The classical *range tree* by Bentley [7] is a two-level data structure: the input points are first stored in a balanced binary search tree sorted by x -coordinate. For each internal node, a secondary tree is built over the y -coordinates of the points in its subtree. This structure supports orthogonal range queries in worst-case $O(\log^2 n + k)$ time, and updates in $O(\log^2 n)$ time. The range tree requires $O(n \log n)$ space. The *k-d tree*, proposed by Bentley and Saxe [6], is a binary search tree that alternately splits space along the coordinate axes. It is simple and practical, with expected query time $O(\sqrt{n} + k)$ in two dimensions [13]. However, its worst-case performance is linear in n . The *quadtree*, introduced by Finkel and Bentley [12], recursively partitions the plane into four quadrants. For uniformly distributed inputs, quadtrees support approximate range queries in expected $O(\log n + k)$ time. Their performance degenerates with clustered data and the worst-case performance is linear in n . We discuss more related work on quadtrees (and Morton encodings) in Section 2.3. The *R-tree* [16] is a balanced, hierarchical data structure widely used in spatial databases. It recursively groups objects into minimum bounding rectangles, forming a tree from bottom to top. *R-trees* perform well

in practice, with expected query and update time $O(\log n + k)$, but their worst-case query time is $O(n)$.

Optimising R-trees. Due to their practical performance, numerous strategies have been proposed to improve the efficiency of *R-trees*. Intuitively, each node in an *R-tree* stores a bounding rectangle that encloses several child rectangles. When a node contains too many children, it is split into two new nodes using a specified *split strategy*. Different *R-tree* variants implement different heuristics for choosing the split: *Linear R-trees* select two entries that are farthest apart and they guarantee that these two elements are in different new nodes (partitioning the remaining children across these two new nodes). This strategy typically has the fastest construction and update times, but yields poorer query performance. *Quadratic R-trees* choose the pair of children whose combination would cause the most overlap, attempting to separate them. This improves query efficiency over the linear variant at the cost of increased insertion time. The *R*-tree* [5] uses a more complex strategy that includes reinserting entries when a good split cannot be found. Although more costly to build and update, this variant improves query performance.

Space-filling curves. A *space-filling curve* (SFC) is a bijective mapping from a one-dimensional interval to a higher-dimensional space. An SFC is *locality-preserving* if consecutive points are nearby in the metric space. The classic example is the Hilbert curve [17]. Locality-preserving SFCs can improve both the static and dynamic performance of *R-trees*. During construction, the input can be sorted along the SFC, and then inserted into the *R-tree* in that order. Because consecutive nodes along the curve are nearby, they tend to be placed into the same leaf nodes. This leads to smaller, tighter minimum bounding rectangles, which improves both query and update efficiency. Additionally, the spatial coherence induced by the SFC improves cache performance for the construction and queries.

1.2 Related implementations. CGAL [11] is the primary library for geometric algorithms. It provides a range tree, *k-d tree* and *R-tree* implementation. The Boost geometric library [8] is a highly optimised geometric algorithms library. It includes three *R-tree* variants using a linear, quadratic, or *R** packing strategy, respectively. Internally, these approaches use Hilbert curves for their construction to improve performance. Boost offers the fastest queries and updates across all existing solutions. It will be our primary comparison. By comparing to these libraries, we compare to all standard data structures and libraries. We do not compare against quadtrees for intricate reasons (we refer ahead to Section 2.3).

Outside of standard libraries, we are aware of five

papers that discuss (rectangular) range query implementations. Kriegel and Schiwietz [22] benchmarked in 1989 the state-of-the-art range reporting approaches. Whilst this result is old, it provided the framework for synthetic data testing that was adopted by future works [2, 28, 33, 26]. The next two works [28, 33] largely consider parallel performance. Sun and Beloch [28] present a parallel framework for iterating over data by using what they call augmented maps. Their `range_tree` class supports improved rectangular range queries, augmented by maps that directly index into a range tree. They claim to also provide faster sequential queries and construction than CGAL and Boost. Wang et al. [33] present a parallel library for geometric algorithms that includes a k - d tree. They compare their k - d tree to a self-made sequential tree, but not to existing libraries or other data structures.

The last two works focus on I/O operations rather than runtime performance. Arge et al. [2] provide an R -tree implementation that is designed to minimise the number of I/O operations performed. Qi, Tao and Chang [26] follow up this work, providing several R -tree implementations that are also designed to minimise the number of I/O's used. The experimental setup in these paper differs from previously discussed work as they measure the number of block I/O operations their data structures use (using a block size of 4MB). They do not optimise for runtime performance. In terms of runtime, they do not compare to (and are not competitive with) the aforementioned implementations.

1.3 Technical contribution. In the plane, Asano, Ranjan, Roos, and Welzl [3] define for a bounding box $D \subset \mathbb{Z}^2$ a *recursive space-filling curve* (RSFC) as a bijection between $[0, \#D] \cap \mathbb{Z}$ and D , with $\#D$ the number of grid points in D , that satisfies two properties: (i) there exist 4 disjoint equal-sized squares covering D such that the inverse of each square is a contiguous interval, and (ii) the restriction of the SFC to each such square is itself an RSFC. Asano et al. [3] prove the following (Fig. 1.1): for any RSFC in \mathbb{R}^2 and for any query square Q , there exist at most $\mu \leq 4$ squares H_1, \dots, H_μ such that: (a) the union $\bigcap_i^\mu H_i$ covers Q , (b) the total area of the H_i is at most 2μ times the area of Q , and (c) the inverse of each H_i is a contiguous interval. They briefly note that this has practical applications. Their contribution is theoretical, as they show the existence of a RSFC with $\mu = 3$ and they prove that this is optimal.

Our paper revisits their technique. We provide a simplification, an implementation, and extensive experimental evaluation of distance query structures. We first restate the result by Asano et al. [3] in terms of quadtrees – generalising their approach to \mathbb{R}^d . Let P be a point set in $D \subset \mathbb{Z}^d$, and let π denote the inverse

of a RSFC that maps D to $[0, \#D] \cap \mathbb{Z}$. Our quadtree defines a RSFC such that $\mu = 2^d$. We construct a static data structure by sorting $p \in P$ by $\pi(p)$ and storing the result in an array A_P . Given a distance query (q, δ) , we compute at most 2^d hypercubes H_1, \dots, H_{2^d} . Each $H_i \cap P$ corresponds to a contiguous interval in A_P , and all points of P within distance δ of q are guaranteed to lie in one of these intervals. This thereby reduces the distance query to 2^d linear scans. One of our main technical contributions is an explicit algorithm for computing these intervals. If P is uniformly distributed, and since the combined volume of the H_i is at most 2^{d+1} times that of Q , the expected overhead is at most a factor 2^{d+1} compared to the optimal. In the worst case, the overhead can be linear. We make our result dynamic in Section 2.2.

On novelty. The core idea of using SFC for range reporting is not new. The earliest work we are aware of is by Tropf and Herzog [31], who describe range reporting techniques over data sorted by Morton codes. Across multiple communities, including spatial databases, computer graphics, and scientific computing, there are several papers that demonstrate awareness of the efficiency gained by combining range reporting with SFCs [18, 23, 24, 27]. Moreover, the benchmark by Qi, Tao and Chang [26] explicitly considers different SFC packing strategies for R -trees. However, in all of these cases, the SFC is used to assist in the construction of more complex data structures, such as R -trees, octrees, or pointerless spatial trees. To the best of our knowledge, there exists no works that use the sorted order along an SFC as a standalone data structure for distance queries.

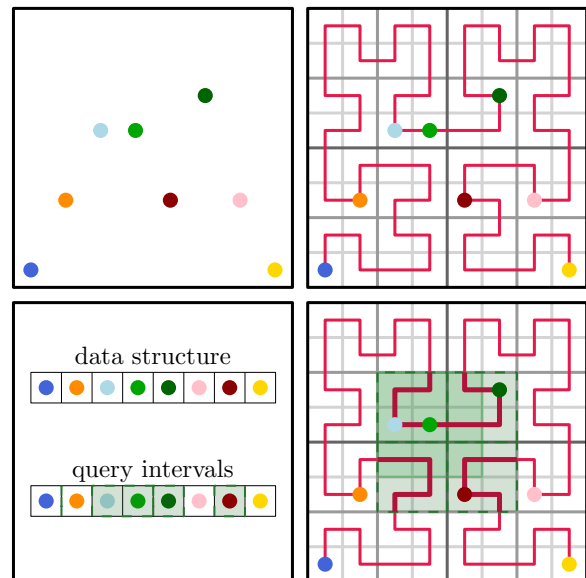


Figure 1.1: The Hilbert curve visits the quadtree cells in a fixed order, thereby providing an ordering of the input.

1.4 Experiments and results. We implement both static and dynamic versions of our technique in two dimensions, using the Hilbert and Z-curves. Our Z-order implementation easily generalises to \mathbb{R}^d via d -dimensional Morton encodings. We compare our method against the state-of-the-art planar range reporting structures. Additionally, we observe that many modern algorithms use range reporting as a subroutine [1, 9, 14, 15, 19, 32, 34]. While a complete survey is beyond our scope, we zoom in on a recent work by van der Hoog et al. [32], who perform trajectory clustering under the Fréchet distance. To create a realistic testbed for our algorithms, we isolate their data set and distance queries and use it as a benchmark.

Results and contribution. Through a variety of real-world data sets, clustering benchmarks and synthetic data sets we evaluate static and dynamic performance of modern distance query structures and our approach. We compare our approach to the CGAL library, the highly-optimised Boost geometric library, and the recent PAM library by Sun and Blöchl [28]. In Section 3 we briefly explain that all other implementations are not competitive in our sequential test setting.

In a static setting, the primary benefit of our `Curve` method is that it is considerably simpler. It frequently offers faster construction times on large data and natively uses less memory since it stores only P in an array. For queries, our `Curve` method is competitive with the highly optimised Boost libraries and it outperforms CGAL [11] and PAM [28]. We additionally observe that on our tests, PAM is a significantly sequentially slower than CGAL and Boost. On query sets with many empty queries, the Boost R -trees become the preferred method because they can terminate early. We note that the three implementations of Boost, statically, have near-identical performance. We thereby argue that their performance primarily comes from their ordering along a SFC and not the surrounding structure.

In a dynamic setting, the Boost structures differentiate themselves. This supports our conjecture that the static R -trees are fast due to their construction along a SFC. The PAM and CGAL libraries are dynamically not competitive. Our approach is dynamically considerably faster: providing a median speedup of a factor 4.5 and 2.1 for insertions and queries compared to Boost.

We thus show a simple but practically efficient technique for distance queries. We match the state-of-the-art in a static setting, and outperform in a dynamic setting. Our experiments thereby support a perhaps surprising conclusion: whilst several sophisticated data structures use space-filling curves to accelerate their performance, the simple act of sorting the input point set P along such a curve is practically sufficient.

2 Space-filling curves and data structure.

In full generality, a *space-filling curve* (SFC) is a bijection from a one-dimensional interval to a higher-dimensional space. In the context of computer science, however, we deal with discrete and bounded domains due to finite precision. Following Asano et al. [3], we assume that our domain D is the integer grid $[1, 2^\omega]^d \cap \mathbb{Z}^d$ (ω denotes the number of bits per coordinate).

PROBLEM STATEMENT 1. *Our input is a point set $P \subseteq [1, 2^\omega]^d \cap \mathbb{Z}^d$. We wish to store P to support distance queries. Each query consists of a point q and a radius δ , and the goal is to return all points in $P \cap B_\delta(q)$, where $B_\delta(q)$ denotes the ball of radius δ centered at q .*

Recursive space-filling curves. Since the domain D in [3] is finite and discrete, an SFC can be regarded as an ordering of $D = [1, 2^\omega]^d \cap \mathbb{Z}^d$. Asano, Ranjan, Roos, and Welzl [3] propose a heuristic for answering distance queries efficiently using a *recursive space-filling curve* (RSFC). We present and implement their approach. First, we show their two-dimensional definition. We then propose an equivalent, generalised formulation which is easier to implement.

DEFINITION 2.1 (RSFC in [3]). *Let D be a square domain in \mathbb{Z}^2 containing m grid points, where m is a power of two. A space-filling curve σ is recursive if there exist four equal-sized squares S_1, S_2, S_3, S_4 such that:*

- *The first $m/4$ points of σ are contained in S_1 , the next $m/4$ in S_2 , and so on.*
- *$\forall i$, the restriction of σ to S_i is itself a RSFC.*

We show an equivalent definition using quadtrees, and we recreate the results in [3] through that definition.

DEFINITION 2.2 (Complete quadtree). *Let $F \subseteq \mathbb{R}^d$ be a hypercube whose diameter is a power of two. The complete quadtree T_F is defined recursively as follows:*

- *If F is not a unit cube, partition F into 2^d equal-sized hypercubes, which become the children of F .*
- *Recurse on each child to construct the full tree.*

A level T_F^ℓ of T_F consists of hypercubes of diameter 2^ℓ .

DEFINITION 2.3 (RSFC in \mathbb{Z}^d). *Let the domain D be a hypercube in $[1, 2^\omega] \cap \mathbb{Z}^d$ with diameter 2^ω . Let F equal D , translated by $-\frac{1}{2}$ in each cardinal direction.*

A recursive space-filling curve π over D is a function that assigns, for all levels $\ell \in [\omega]$, to each cube $C \in T_F^\ell$ a unique bit string $\pi(C)$ of length $d \cdot \ell$, s.t.:

- *Each cube C has a unique string $\pi(C)$, and*
- *$\forall C' \in T_F$ with $C' \subset C$, $\pi(C)$ is a prefix of $\pi(C')$.*

Our RSFC π assigns $\forall p \in D$ the value $\pi(p) := \pi(C)$, where C is the unique unit cube in T_F containing p .

LEMMA 2.4. *There is a one-to-one correspondence between the orderings σ of D from Definition 2.1 and the mappings π of D from Definition 2.3.*

Proof. Consider a recursive space-filling curve σ as in Definition 2.1. Its recursive subdivision of D into equal-sized squares induces a quadtree. We construct a mapping π satisfying Definition 2.3 in a top-down fashion. Each internal tree node has four children S_1, S_2, S_3, S_4 such that all points of σ in S_1 precede those in S_2 , and so on. We assign to S_1, S_2, S_3, S_4 the binary suffixes 00, 01, 10, and 11, respectively. The code $\pi(S_i)$ is defined as the parent’s code concatenated with the appropriate suffix. This results in a unique map π for every σ that satisfies Definition 2.3. Conversely, given a map π over a $D \subset \mathbb{Z}^2$ (with diameter a power of two) that satisfies Definition 2.3, we can induce a total order σ on $D \cap \mathbb{Z}^2$ by sorting the points $p \in P$ by $\pi(p)$. This produces an ordering σ satisfying Definition 2.1. \square

Distance queries. Definition 2.3 allows for a new formulation and implementation of the distance query heuristic by Asano et al. [3]. Each point $p \in P$ is assigned a bitstring $\pi(p)$ of length $d \cdot \omega$. For any hypercube $C \in T_F$, we define $\pi(C) \circ \bar{0}$ as the string obtained by appending zeroes to $\pi(C)$ until the total length is $d \cdot \omega$; we define $\pi(C) \circ \bar{1}$ analogously.

OBSERVATION 1. *For any $C \in T_F$ and any point $q \in C \cap \mathbb{Z}^d$, we have: $\pi(C) \circ \bar{0} \leq \pi(q) \leq \pi(C) \circ \bar{1}$.*

DEFINITION 2.5. *Given a query hypercube Q , we define $\text{cells}(Q)$ as the hypercubes $C_i \in T_F$ satisfying:*

- $|Q| \leq |C_i| < 2|Q|$, and $C_i \cap Q \neq \emptyset$.

Let A_P be an array storing all $p \in P$, sorted by increasing $\pi(p)$. Then the distance query heuristic (see Algorithm 2.1) proceeds as follows: Given a query (q, δ) , compute the smallest axis-aligned hypercube Q that contains $B_\delta(q)$. Compute $\text{cells}(Q)$ as defined above. For each $C_i \in \text{cells}(Q)$, perform a binary search on A_P to find the subarray between $\pi(C_i) \circ \bar{0}$ and $\pi(C_i) \circ \bar{1}$. Then iterate over each point p' in that subarray, returning those for which $\|p' - q\| \leq \delta$.

Efficiency. The union of all cubes in $\text{cells}(Q)$ covers a region whose volume is at most $2 \cdot 2^d$ times that of Q . At first glance, this may suggest inefficiency. In the worst case, $\Theta(n)$ points could lie within $\text{cells}(Q)$ even if Q itself contains no points from P , yielding an $O(n)$ additive overhead. However, several practical factors mitigate this cost: First, the algorithm iterates only over the points in P , not the entire grid. Thus if P is sparse, then $\text{cells}(Q) \cap P$ is likely to be small. Secondly, all range scans occur over contiguous memory, leading to highly efficient cache behaviour—often outperforming structures like binary search trees in practice.

Algorithm 2.1 Query(point q , distance δ , array A_P)

```

 $Q \leftarrow$  bounding box  $B_\delta(q)$ .
output  $\leftarrow \emptyset$ 
for  $C_i \in \text{cells}(Q)$  do
   $x \leftarrow A_P.\text{lower\_bound}(\pi(C_i) \circ \bar{0})$ 
  while  $\pi(A[x]) < \pi(C_i) \circ \bar{1}$  do
    if  $\|A[x] - q\| < \delta$  then
      output.append( $x$ )
     $x++$ 
return output

```

2.1 Implementation details. Let the domain D and F be fixed. Algorithm 2.1 yields a simple and lightweight heuristic for answering distance queries. We now describe a few implementation details.

Choice of RSFC. Asano et al. [3] initially consider the Hilbert curve. They then provide a theoretical construction of a recursive space-filling curve (RSFC) in two dimensions that guarantees the number of unique elements in $\text{cells}(Q)$ is at most three, rather than four. However, we note that although this improves the number of binary searches needed, and may reduce the total volume of the region considered, their function is complicated to implement.

The Hilbert curve is widely used in data structures because it is locality-preserving: all pairs of consecutive points along the curve have distance at most two. This property is exploited to speed up range reporting structures, including the R -trees in Boost [8]. We therefore include a Hilbert-curve implementation. Concretely, we implement the function π from Definition 2.3 such that the ordering of D by π follows a Hilbert curve.

However, in our specific application, the locality-preserving property of the Hilbert curve is not exploited. Distance queries are handled purely by binary search and direct scanning. Therefore, we also offer a second implementation using the Z-curve (also known as the Morton curve). The Z-curve has an additional practical property: for any point $q \in N$, the bit-string $\pi(q)$ can be computed efficiently by interleaving coordinate bits. That is, the bit pairs in $\pi(q)$ can be constructed independently (see Algorithm 2.2).

Storing P twice. To accelerate binary search during queries, we store the point set P in two separate arrays. The array A_P stores the elements of P sorted by their π -values. The second array B stores the corresponding bit strings: for all indices i , we define $B[i] = \pi(A[i])$.

This preprocessing avoids computing $\pi(p)$ during queries. In particular, the binary search step¹ becomes a direct comparison over the entries of B .

¹specifically, $A_P.\text{lower_bound}(\pi(C_i) \circ \bar{0})$ in Algorithm 2.1

Algorithm 2.2 Z-curve $\pi(\text{point } p \in [2^\omega]^2)$

```
output  $\leftarrow$  string[ $2\omega$ ]  
for  $i \in [\omega]$  do  
    output[ $2i$ ]  $\leftarrow$  the  $i$ 'th bit of  $p.x$   
    output[ $2i + 1$ ]  $\leftarrow$  the  $i$ 'th bit of  $p.y$   
return output
```

2.2 Dynamic implementation. There are two ways that our data structure can trivially be made dynamic. Firstly, one could store all $p \in P$, sorted by $\pi(p)$, in a balanced tree. Our repository offers an implementation using a B-tree. This method provides fast updates (inserting a point into a sorted subsequence is a fast operation) but it is inefficient in queries. This is because in a balanced tree, consecutive leaf values can no longer be guaranteed to be consecutive in memory. Secondly, we observe that a distance query is decomposable. This allows us to obtain an efficient insertion-only implementation through the logarithmic method by Overmars [25]. Our repository contains the insertion-only implementation that we use for our experiments. In practice, the logarithmic method can be made fully dynamic through the tombstoning technique [20].

2.3 Quadtrees. Algorithm 2.2 implements what is commonly known as the Z-curve, or Morton, encoding. These are widely used in quadtrees, as they provide an efficient means to determine, for any point q and quadtree level ℓ , a bit string that uniquely identifies the hypercube at level ℓ containing q . This property enables the use of quadtrees without pointers [10, 29, 30, 35, 36].

A quadtree supports distance reporting queries as follows: Given a query (q, δ) , it computes the smallest axis-aligned hypercube Q that contains the ball $B_\delta(q)$. It then identifies all nodes at level $\lceil \log \|B_\delta(q)\| \rceil$ that intersect Q . For each such node C , it traverses its descendant leaves and reports the points in those leaves that lie within $B_\delta(q)$. By Definition 2.3, Lemma 2.4 and Algorithm 2.1, we thereby show that process is equivalent to the heuristic proposed by Asano et al. [3].

There is a crucial distinction: our quadtree is purely conceptual. We neither construct nor traverse a tree. Instead, we operate solely on a sorted array. While quadtree distance queries follow the same high-level logic, they do so in an involved and less efficient manner:

- Regular quadtrees incur significant overhead because leaves are not stored contiguously.
- Pointer-free quadtrees use hash maps or dictionaries to map Morton codes to quadtree nodes [29, 35, 36], which introduces a significant lookup overhead.
- Karras [18] lays out quadtree cells in an array such a Morton codes directly address the corresponding

quadtree cells. However, this approach still stores the entire tree. In contrast, we store only the leaves: i.e., the point set P sorted along the Z-curve.

In essence, our queries execute the same logic as quadtree queries. As such, we argue that a performance comparison against quadtrees primarily reflect implementation overheads, not fundamental algorithmic differences. In addition, quadtrees are typically implemented to support nearest-neighbour queries. We are not aware of any implementation that claims to outperform R -trees. Typically, R -trees have better performance than quadtrees [21], which is also illustrated by Boost using R -trees. We therefore do not include quadtrees in our experiments.

3 Experimental setup.

We conduct a range of experiments to measure the performance of distance query data structures. At a high level, we perform four types of experiments.

First, following established precedent in range reporting [26], we evaluate all range-reporting solutions on the real-world **Tiger** and **TigerEast** data sets. Second, we consider an application domain: a recent subtrajectory clustering implementation [32] where distance queries dominate the running time. We isolate the data structure construction and queries and use them as a benchmark. This allows us to assess performance in a realistic setting, and it allows us to use additional real-world data: the trajectory data used in a clustering application. Third, we measure construction and query performance on synthetic data. Synthetic data enables controlled experiments at larger input sizes and facilitates asymptotic analysis. Finally, we evaluate dynamic behaviour on synthetic data by, for varying input sizes n , first inserting n points and then performing n queries.

We provide a test suite for running experiments, generating synthetic data, and plotting results at [4]. We ran experiments on a machine with a 4.2 GHz AMD Ryzen 9 7950X3D and 128 GB of memory.

3.1 Algorithms.

- We compare the following:
0. **Curve-H:** Our data structure using a Hilbert curve.
 1. **Curve-Z:** Our data structure using a Z-curve.
 2. **CGAL-R:** A CGAL implementation of a Range tree.
 3. **CGAL-KD:** A CGAL implementation of a Kd tree.
 4. **Boost-L:** A Boost r-tree with linear packing.
 5. **Boost-Q:** A Boost r-tree with quadratic packing.
 6. **Boost-R*:** A Boost r-tree with R* packing.
 7. **PAM-R:** the map-augmented Range tree from [28].

We note that this excludes the data structures from [2, 26, 33]. We explain why: the data structures from [2, 33] optimise for I/O's rather than runtime, and they are not

competitive on runtime. The algorithms from [33] consider parallel computations and the scope of this paper is sequential computations. Moreover, the data structure from [33] is not sequentially efficient (the authors themselves also do not claim it to be). Sun and Blelloch [28] in full generality present a multi-threaded algorithm. However, they also claim a superior sequential performance over Boost and CGAL. We therefore include the algorithm from [28], but we explicitly restrict it to run sequentially to stay within our sequential scope.

3.2 Data sets.

Real-world data. We follow precedent [26] and use the **Tiger** data set, which consists of geographical features from the US Census Bureau’s system. We also use the smaller **TigerEast** data set. These sets contain 35,904,948 and 17,468,291 points respectively.

Real-world trajectories. We additionally evaluate performance in the application domain of subtrajectory clustering [32]. This algorithm computes a clustering of (sub)trajectories by issuing a large number of distance queries. Their performance is dominated by the distance query time. We first ran their algorithm, isolating the input points P and the set of distance queries \mathcal{Q} . We then use this input as a benchmark where we measure the total time of constructing a data structure on P and executing all queries in \mathcal{Q} . We argue that our benchmark issues a ‘realistic’ measurement in the sense that the computations directly arise during a clustering algorithm. We feed this benchmark three real-world data sets: the **Athens-small**, **Berlin**, and **Chicago** data sets from mapconstruction.org of, respectively, 2,840, 192,223, and 118,360 points. We note that [32] subsample the **Berlin** and **Chicago** by a factor 10 and 4, respectively. We also include these subsampled versions.

Synthetic data. We measure asymptotic scaling, following [22, 26], using synthetic data. Our data generators take as input a square bounding box. Synthetic data is parameterised by the bounding box size, input size, and the distribution from which the data is sampled. The size of the bounding box Δ determines the number of bits per variable. It thus affects the efficiency of our space usage and access patterns. Our program can facilitate $\Delta \in \{2^8, 2^{16}, 2^{32}\}$. The input size n is chosen from $n \in \{0.5M, 1M, 5M, 10M, 20M, 40M\}$. Note that for fixed n , smaller Δ yields a denser point set. For fixed (Δ, n) , we generate points from four distributions:

0. **Uniform:** uniformly random sampling.
1. **Gaussian:** 2D Gaussian sampling $(\mu, \sigma) = (\frac{\Delta}{2}, \frac{\Delta}{8})$.
2. **Skewed:** x -coordinates are sampled uniformly; y -coordinates follow a geometric distribution [2, 26].
3. **Clustered:** \sqrt{n} centres are uniformly generated. Around each centre we generate \sqrt{n} points from a 2D Gaussian distribution $(\mu, \sigma) = (0, \frac{\Delta}{100})$ [2, 22].

3.3 Queries. For any data set, outside of our clustering benchmark, we randomly generate L_∞ distance queries. All methods perform a distance query (q, δ) by performing a square query Q such that $B_\delta(q) \subseteq Q$, followed by a filtering step to output only points in $P \cap B_\delta(q)$. Thus, the specific choice of metric has marginal to no impact on relative performance. Query generation follows [22, 26], using two parameters. The first parameter is the relative query size ρ . Queries consist of a centre q and a diameter $\delta = \rho \cdot \Delta$. Smaller ρ values correspond to smaller expected result sets. We follow [22, 26] and choose $\rho \in \{0.001, 0.01, 0.02\}$ (a strict subset of the values considered in [26]). The centre q is sampled from one of our four distributions.

3.4 Experiment configuration. For our synthetic data sets, we define *synthetic configurations*:

DEFINITION 3.1. A synthetic configuration fixes a data structure, bounding box size Δ , one of the four input distributions, query size ρ , and query distribution. For $n \in \{0.5M, 1M, 5M, 10M, 20M, 40M\}$ we measure:

- Construction time: the time taken by the static construction algorithm on a point set P of size n .
- Query latency (ms/query): measured by a throughput experiment where we perform as many queries as possible within $\min\{\frac{n}{10^6}, 10\}$ seconds.

We repeat each run 3 times and report the median.

We note that our throughput experiment is performed by batching the query streams. After each batch, we verify how much time has elapsed and if we exceed the time limit, we terminate. We then divide the actual time used by the number of queries performed to receive the number of queries per (milli)second.

Restricting synthetic configurations. Our parameter choices define $8 \cdot 3 \cdot 4 \cdot 3 \cdot 4 = 1152$ possible synthetic configurations (twice as many if we consider static and dynamic variants). Even with the throughput experiment limited to 10 seconds, each configuration requires up to 18 minutes to run. Running all configurations with only static algorithms would already require 14.4 days. We restrict the configurations by fixing $\Delta = 2^{16}$ to get a more manageable 384 static experiments. This choice mirrors [22], which used 16 bits per coordinate (yielding the same density for fixed n). Qi, Tao and Zhang [26] sample doubles uniformly in $[0, 1] \times [0, 1]$ and refine precision until points are distinguishable, corresponding to approximately 20 bits per variable. Their approach can therefore be rescaled to a bounding box of $[0, 2^{20}] \times [0, 2^{20}]$, which is comparable to our setup. In the paper writeup, we additionally choose $\rho = 0.01$ but our repository contains zip files with the full set of experimental results. In Section 7 we discuss the relative impact of different query and bounding box sizes.

Dynamic experiments. The key difference in our dynamic experiments is that, for each fixed n , we insert n points dynamically. We then perform our query throughput experiment. Deletions are not tested.

Plots and discussion. Throughout the paper, PAM-R, CGAL-KD and CGAL-R are frequently so slow that we exclude them from the plots and discussion. Also, CGAL-KD use lazy initialisation and we can therefore not discuss their construction or insertion time. Appendix D contains tables with all algorithmic results.

4 Real-world and trajectory data.

We evaluate static performance on two types of real-world data: the **Tiger** datasets, and trajectory data. For the latter, we run our the benchmark that we derived from [32]. Our benchmark receives a set of trajectories and generates a collection of queries by running the clustering algorithm from [32]. These two data sources induce distinct experimental behaviours. The **Tiger** datasets consist of scattered points across the USA, with large regions of empty space. When using random query centres, this naturally leads to many empty distance queries. In contrast, the trajectory data contains numerous overlapping points, never generates empty queries, and it issues exactly n queries. We elaborate further on these distinctions in Appendix A.

Clustering benchmark. Figure 4.1 shows results on the benchmark derived from [32]. All three Boost libraries deliver near identical performance and are consistently the fastest. In contrast, the range trees CGAL-R and PAM-R are significantly slower. This is in line with expectations: Range trees are pointer-based and store their leaves in a non-consecutive manner. Both data structures are significantly bottlenecked by pointer traversals and I/O's. CGAL-KD remains competitive for smaller datasets but fails to scale as well as other techniques. Finally we note that the Curve methods perform reasonably well on this data: they are between $1.19\times$ and $2.4\times$ slower than Boost, with the performance gap decreasing as dataset size increases.

Tigers. Figure 4.2 shows construction times on **Tiger** and **TigerEast**, and query times on **Tiger**. Curve-Z achieves the fastest construction times, while Curve-H is noticeably slower. CGAL-R and PAM-R are again outliers in performance as CGAL-R even times out. In terms of query performance, the Curve methods and CGAL-KD are highly competitive. Boost, however, are *very* fast on this data achieving under 0.00005 ms per query – a factor 3.67-37.12 faster than Curve-Z. This speedup is particularly present on **Gaussian** queries, as the centre of the distribution lies in an empty region of the dataset. This behaviour illustrates a recurring trend: R-trees can terminate early on empty queries, and this greatly impacts their performance.

Reflection. Contrary to the findings in [29], we find that PAM-R lags significantly behind. The remaining relative performance is context-dependent. In static settings with empty queries, Boost's R-tree variants dominate. On smaller input sizes, CGAL-KD remains competitive. In workloads with larger n , or where construction time matters, our Curve approach provides a simple and effective alternative. Finally, we observe that all Boost variants perform nearly identically, despite their differing tree heuristics. We conjecture that their SFC (and early terminations) delivers most of their performance, rather than their respective tree structures.

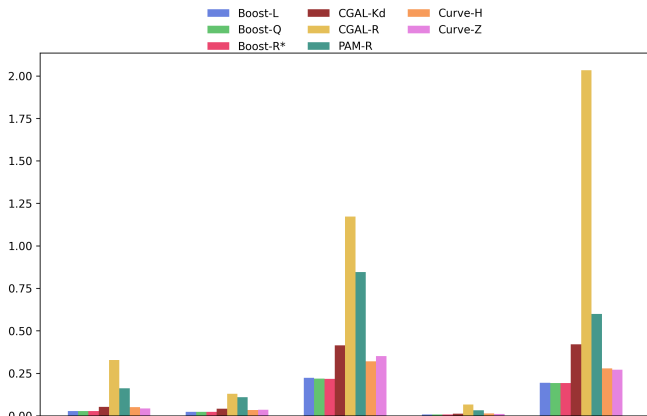


Figure 4.1: Total runtime (s) of the clustering benchmark.

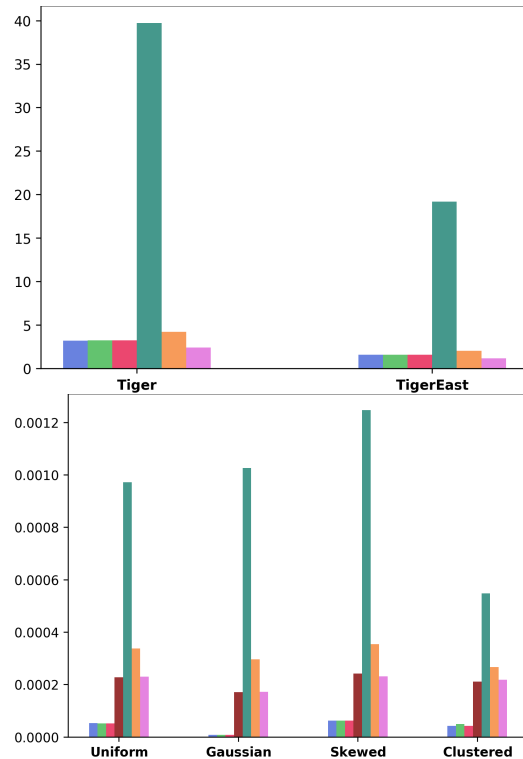


Figure 4.2: Top: Construction time (s). Bottom: query times (ms) on **Tiger**. PAM-R is teal.

5 Static synthetic experiments.

We evaluate the asymptotic behaviour of the eight static versions of all data structures. We measure construction time and query latency. Data sets are generated from four distributions within a bounding box of diameter $\Delta = 2^{16}$. Queries are generated from four distributions, with query diameter $\rho\Delta$ for $\rho \in \{0.001, 0.01, 0.02\}$. This results in 384 configurations (Definition 3.1) where each configuration tests a single algorithm for six values of n , three times. All results are available in the project repository. We observe that **CGAL-KD**, **CGAL-R** and **PAM-R** are considerably slower for larger n . They are therefore excluded from the plots and discussion but we include them in Appendix D.3.

5.1 Static construction. The ranking of the remaining static algorithms is consistent across all input distributions: **Curve-Z** achieves the fastest construction times, whilst **Curve-H**, **Boost-R***, **Boost-Q**, and **Boost-L** are near-indistinguishable. The relative performance gap between solutions varies by data set, but they all share the same trends. Figure 5.1 presents results for the **Clustered** data set, where algorithmic differences are most pronounced. **Curve-Z** does not exploit specialised bit-tricks for computing Z-order (Morton) encodings. Yet, evaluating the Z-ordering function is already substantially faster than the Hilbert curve computation. **Curve-Z** always outperforms Boost and **Curve-H** is either comparable or faster. The performance gaps widen with increasing input size. At the largest input size ($n = 40M$), **Curve-Z** is a factor 1.46-1.73 faster than Boost. Appendix B provides further discussion. In addition to these observations, we wish to briefly note that sorting is trivially parallelisable. Appendix B.3 discusses the effect of parallel sorting on construction times for our **Curve** methods.

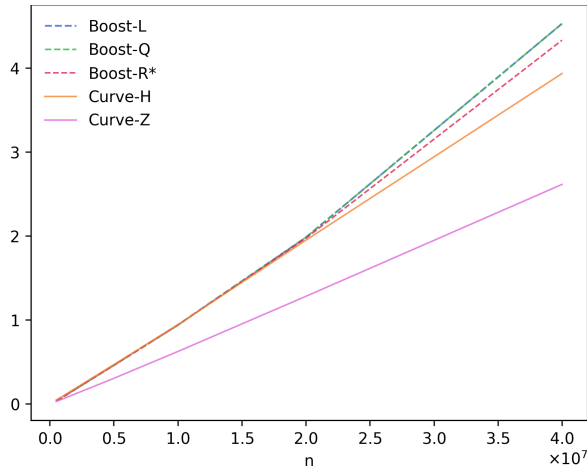


Figure 5.1: Construction time (s) on **Clustered** data within a bounding box of $\Delta = 2^{16}$ for increasing input size n .

5.2 Query latency. The data set has only a marginal effect on query performance. In contrast, the query distribution has a significant impact. When query centres are sampled from a **Uniform** distribution, query performance is nearly indistinguishable. For **Gaussian** and **Skewed** distributions, performance remains similar, though the Boost implementations exhibit better asymptotic scaling (Figure 5.2 (top)). Nonetheless the performance always lies within a factor 0.96-2.07. The median speedup provided by Boost is a factor 1.56.

However, when query centres follow a **Clustered** distribution, the Boost implementations are significantly faster (Figure 5.2 (bottom)). We attribute this performance gain on **Clustered** queries to the R-tree’s ability to terminate early when queries are empty. If an R-tree encounters an empty bounding box near the root, it terminates in constant time. In contrast, our methods based on binary search must fully execute all four binary searches regardless of query outcome. This hypothesis is supported by additional experiments where we enlarge the bounding box, thereby increasing the likelihood that queries return empty results.

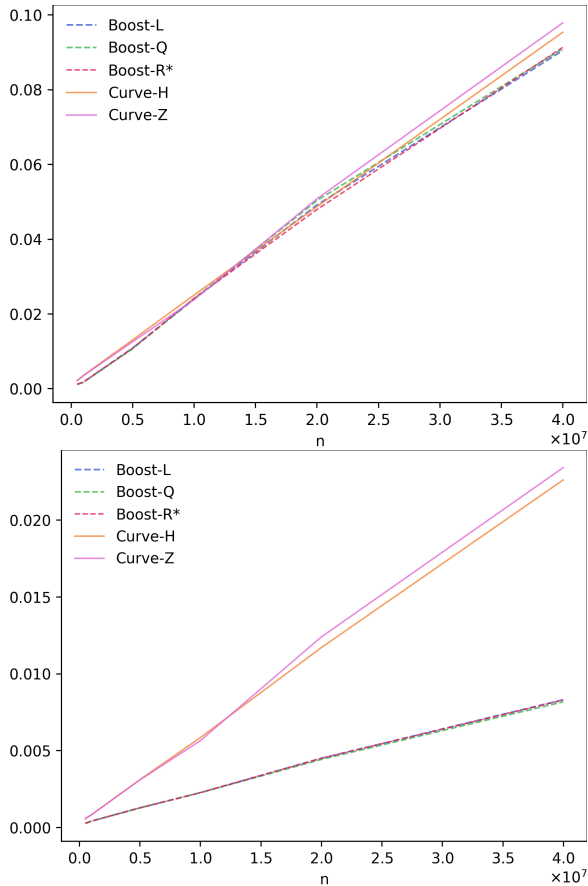


Figure 5.2: Query latency (ms) on **Gaussian** data for increasing n . Queries are generated using a **Gaussian** (top) or **Clustered** (bottom) distribution and $\rho = 0.01$.

6 Dynamic synthetic experiments.

We evaluate dynamic asymptotic behaviour. Specifically, we measure insertion and query times. As previously explained, our **Curve** method can be made dynamic in two straightforward ways: either by storing the sorted point set in a balanced search tree, or by using the logarithmic method of Overmars [25]. Our repository implements both approaches. Local experiments confirm that the logarithmic method is significantly more efficient, and we therefore discuss this version here. Thus, we still compare eight data structures and we use the same 384 synthetic configurations as in Section 5 for our experiments. We note that the performance of **CGAL-KD**, **CGAL-R** and **PAM-R** is considerably worse than the others and we therefore focus on comparing to Boost. Appendix C provides a more detailed discussion of our findings and Appendix D.4 provides the data for all data structures.

6.1 Insertion latency. The insertion time (ms) across all data structures is independent of the underlying data set; Figure 6.1 shows results for the **Uniform** data set, with **CGAL** excluded for clarity. The Boost implementations performed almost identically statically. Yet, they have substantial dynamic performance differences. We conjecture that static *R*-tree construction relies primarily on sorting P along a space-filling curve (SFC). In dynamic settings, this ordering has less impact, leading to greater performance variations. The simpler linear splitting rule is notably faster.

Overall, the **Curve** methods dominate in dynamic insertion performance. As in static construction, the implementation using a **Z**-curve is consistently more efficient than its Hilbert curve counterpart. The insertion time of **Curve-Z** is between a factor 1.50-13.00 faster than the insertion time of any Boost implementation. The median speedup is a factor 4.5. Notably, the performance gap is relatively independent of the input size.

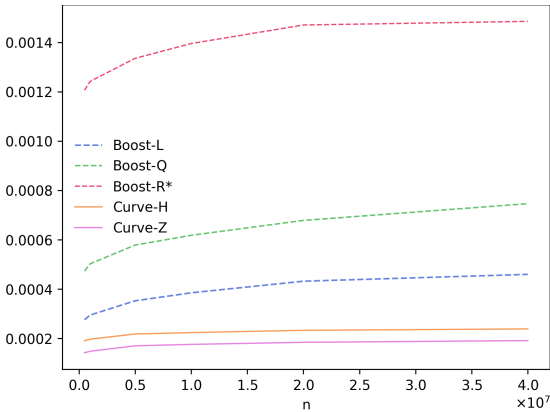


Figure 6.1: Insertion time (ms) on **Uniform** data within a bounding box of $\Delta = 2^{16}$ for increasing input size n .

6.2 Queries. As in the static experiments, the data set has a marginal impact on query performance. The query distribution has a reduced impact. Results on all distributions except **Clustered** queries follow the same trend. Figure 6.2 illustrates query latency.

The Boost implementations exhibit significant differences in performance. As expected, **Boost-R*** is the most efficient among them, while **Boost-L** is the least efficient. The various *R*-tree implementations thereby offer a trade-off between insertion and query efficiency. In contrast to the static setting, the **Curve** methods achieve faster queries than Boost on almost all data sets and query distributions. They consistently provide the best performance (except on **Clustered** data) and best scaling, providing a speedup of a factor 1.65–8.06 on maximum input sizes. The median speedup across all data is a factor 2.10. On **Clustered** data, **Boost-R*** performs best overall, though the **Curve** methods still outperform other Boost variants. We observe that **Boost-Q** appears to scale slightly better than any **Curve** method.

When considering both queries and insertions, our proposed method clearly offers the most efficient solution. Although **Boost-R*** achieves better query performance on clustered query workloads, this advantage is offset by its substantially higher insertion cost.

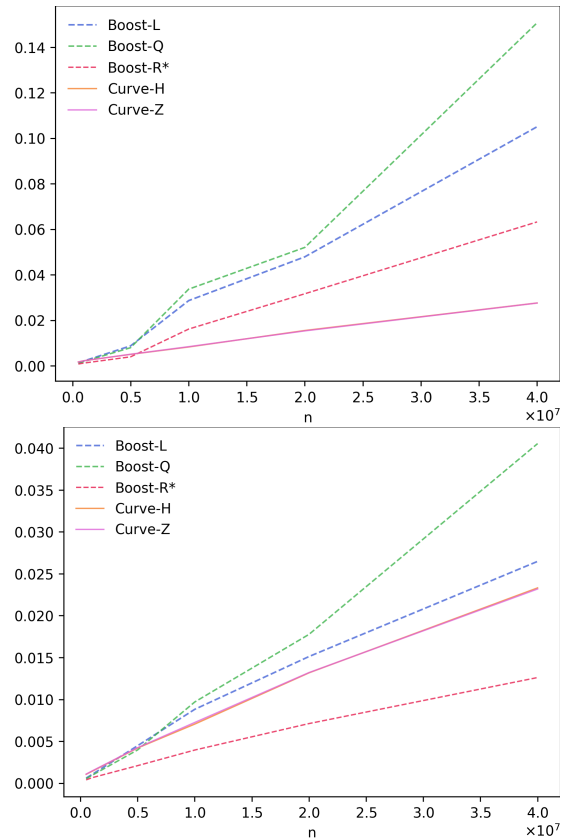


Figure 6.2: Query latency (ms) on **Clustered** data. Queries follow a **Uniform** (top) or **Clustered** distribution.

7 Alternative considerations.

Our experiments compare the efficacy distance query data structures under a range of real-world, trajectory, and synthetic data sets. Naturally, our experiments cannot cover every possible setting. Throughout the main text, we noted several implementation and experimental considerations that we briefly elaborate on.

Real-world data. We considered two types of real-world data: the **Tiger** data and trajectories from mapconstruction.org. For the former, we used synthetic random queries; for the latter, we executed a benchmark that we based on a subtrajectory clustering algorithm from [32]. Our results demonstrate that these two scenarios yield different outcomes: the **Tiger** data contain many sparse regions, resulting in random queries frequently producing empty query ranges. This favours R -trees who can terminate early on empty queries. In contrast, the trajectory data is dense and the clustering algorithm issues queries only from input points, so distance queries are never empty. We find that experimental setups highlight contrasting behaviours of our performance and that they cover a variety of real-world data sets of different sizes. Yet, we do acknowledge that more real-world datasets could be explored.

Other parameters. In the main text, we fixed the bounding box diameter to $\Delta = 2^{16}$ and set the query diameter to $\rho\Delta$ with $\rho = 0.01$. Our repository includes additional results for other values of ρ , and we performed limited experiments for $\Delta \in \{2^8, 2^{32}\}$. Despite presenting a subset of our experiments, clear trends emerge: as point sets become less dense or query windows become smaller, the likelihood of empty queries increases. This benefits R -tree performance. Conversely, our **Curve** data structure becomes more competitive as the bounding box decreases or query sizes increase.

Optimisations. We discussed several algorithmic optimisations in the main text. One consideration is a space-saving variant where we store only P , computing $\pi(p)$ on the fly for each $p \in P$. Our repository includes such a 'no rank' implementation, but this significantly slows query performance.

We can also further optimise Algorithm 2.2, which computes the Z-order rank of a point. This computation is trivially parallelisable. Moreover, some hardware and operating systems offer native instructions for Morton encodings, which could accelerate this step substantially. Since this rank computation is frequently a bottleneck for our approach, we observe that further optimisation is possible. We deliberately refrained from such optimisations to favour the simplicity of our approach. Finally, we briefly note that due to the simplicity of our approach, we can almost immediately generalise to \mathbb{R}^d through d -dimensional Morton encodings.

8 Conclusion.

We proposed a simple and practical data structure for distance reporting queries, based on sorting the input point set along a space-filling curve (SFC). We acknowledge that the underlying idea is not new [3]. Nonetheless, many recent papers favour range reporting over this approach [1, 9, 14, 15, 19, 32, 34]. State-of-the-art range reporting implementations already use SFCs to improve performance, but additionally maintain a traditional structure such as an R -tree, quadtree, or k -d tree as a wrapper. We advocate to discard this surrounding data structure entirely, storing the input points P directly in sorted order instead.

We provide a basic C++ implementation. We then conduct extensive experiments where we compare modern approaches for distance queries. Of note is that we, contrary to [28], observe that PAM-R is, sequentially, significantly slower than its competitors. In static settings, our method achieves very fast queries as we had to suspend comparisons to all data structures except for the highly optimised Boost library. Compared to Boost, we offered competitive performance but the relative performance declines as the number of queries or the fraction of empty queries increases. For construction time, our approach is the fastest, especially if parallelism is allowed. An interesting observation that the *locality-preserving* property of Hilbert curves has no impact on query performance. The fact that a Z-ordering is easier to compute makes this the preferred method.

In dynamic settings, our approach consistently outperforms all competitors in both insertion and query times. We show that PAM-R or CGAL cannot compete with the highly optimised Boost library or our solution. **Boost-R*** offers faster queries when many queries are empty, but this advantage is offset by its significantly slower insertions. Our dynamic experiments also provide insight into R -trees: while their performance is nearly indistinguishable statically, their dynamic performance strongly diverges. We conjecture that the static R -trees rely extensively from ordering points along an SFC at construction time. In dynamic settings, the splitting strategy is less sensitive to this ordering.

We thus demonstrate a simple, practical technique for distance queries, with competitive static performance and superior dynamic performance. Our experiments provide insights into modern distance query implementations, and show that much of their practical efficiency can be achieved by simply sorting along a SFC. Due to its simplicity, our approach can be easily further optimised and it also trivially extends to higher dimensions. An interesting future direction would be to explore whether we can augment our structure with a truncated R -tree to terminate early on empty queries.

References

- [1] M. E. ALI, S. S. EUSUF, K. ABDULLAH, F. M. CHOUDHURY, J. S. CULPEPPER, AND T. SELLIS, *The maximum trajectory coverage query in spatial databases*, Proceedings of the VLDB Endowment, 12 (2018), p. 197–209, <https://doi.org/10.14778/3291264.3291266>.
- [2] L. ARGE, M. D. BERG, H. HAVERKORT, AND K. YI, *The priority r-tree: A practically efficient and worst-case optimal r-tree*, ACM Transactions on Algorithms, 4 (2008), <https://doi.org/10.1145/1328911.1328920>.
- [3] T. ASANO, D. RANJAN, T. ROOS, E. WELZL, AND P. WIDMAYER, *Space-filling curves and their use in the design of geometric data structures*, Theoretical Computer Science, 181 (1997), pp. 3–15, [https://doi.org/https://doi.org/10.1016/S0304-3975\(96\)00259-9](https://doi.org/https://doi.org/10.1016/S0304-3975(96)00259-9).
- [4] A. AUTHOR(S), *Library and Benchmark*. <https://anonymous.4open.science/r/SFC-Index>, 2025.
- [5] N. BECKMANN, H.-P. KRIEGEL, R. SCHNEIDER, AND B. SEEGER, *The r*-tree: an efficient and robust access method for points and rectangles*, in ACM International Conference on Management of Data (SIGMOD), SIGMOD '90, New York, NY, USA, 1990, Association for Computing Machinery, p. 322–331, <https://doi.org/10.1145/93597.98741>.
- [6] J. L. BENTLEY, *Multidimensional binary search trees used for associative searching*, Communications of the ACM, 18 (1975), p. 509–517, <https://doi.org/10.1145/361002.361007>.
- [7] J. L. BENTLEY AND J. B. SAXE, *Decomposable searching problems i. static-to-dynamic transformation*, Journal of Algorithms, 1 (1980), pp. 301–358, [https://doi.org/https://doi.org/10.1016/0196-6774\(80\)90015-2](https://doi.org/https://doi.org/10.1016/0196-6774(80)90015-2).
- [8] BOOST C++ LIBRARIES, *Boost.Geometry (a.k.a. Generic Geometry Library)*, Boost.org, 2024. <https://www.boost.org/doc/libs/release/libs/geometry/>.
- [9] K. BUCHIN, M. BUCHIN, J. GUDMUNDSSON, J. HENDRIKS, E. H. SERESHI, R. I. SILVEIRA, J. SLEIJSTER, F. STAALS, AND C. WENK, *Roadster: Improved algorithms for subtrajectory clustering and map construction*, Computers and Geosciences, 196 (2025), p. 105845, <https://doi.org/10.1016/j.cageo.2024.105845>.
- [10] H. K.-C. CHANG AND C.-Y. LIOU, *Parallel implementation of linear quadtree codes using the ncube 2 supercomputer system*, International Journal of High Performance Computing Applications, 9 (1995), p. 220–231, <https://doi.org/10.1177/109434209500900304>.
- [11] A. FABRI AND S. PION, *CGAL: The computational geometry algorithms library*, Proceedings of the 17th ACM SIGSPATIAL International Conference on Advances in Geographic Information Systems, (2009), pp. 538–539, <https://doi.org/10.1145/1653771.1653865>.
- [12] R. A. FINKEL AND J. L. BENTLEY, *Quad trees a data structure for retrieval on composite keys*, Acta Informatica, 4 (1974), p. 1–9, <https://doi.org/10.1007/BF00288933>.
- [13] J. H. FRIEDMAN, J. L. BENTLEY, AND R. A. FINKEL, *An algorithm for finding best matches in logarithmic expected time*, ACM Transactions on Mathematical Software, 3 (1977), p. 209–226, <https://doi.org/10.1145/355744.355745>.
- [14] J. GUDMUNDSSON, M. HORTON, J. PFEIFER, AND M. P. SEYBOLD, *A practical index structure supporting fréchet proximity queries among trajectories*, ACM Trans. Spatial Algorithms Syst., 7 (2021), <https://doi.org/10.1145/3460121>.
- [15] J. GUDMUNDSSON, J. PFEIFER, AND M. P. SEYBOLD, *On practical nearest sub-trajectory queries under the fréchet distance*, 9 (2023), <https://doi.org/10.1145/3587426>.
- [16] A. GUTTMAN, *R-trees: a dynamic index structure for spatial searching*, in ACM International Conference on Management of Data (SIGMOD), SIGMOD '84, New York, NY, USA, 1984, Association for Computing Machinery, p. 47–57, <https://doi.org/10.1145/602259.602266>.
- [17] D. HILBERT, *Über die stetige abbildung einer linie auf ein flächenstück*, Mathematische Annalen, 38 (1891), pp. 459–460, <https://doi.org/10.1007/BF01199431>.
- [18] T. KARRAS, *Maximizing parallelism in the construction of bvhs, octrees, and k-d trees*, in ACM SIGGRAPH / Eurographics Conference on High-Performance Graphics, EGGH-HPG'12, Goslar, DEU, 2012, Eurographics Association, p. 33–37.
- [19] J. KIM, S. HONG, S. JEONG, S. PARK, AND K. YU, *Sgir-tree: Integrating r-tree spatial in-*

- dexing as subgraphs in graph database management systems*, ISPRS International Journal of Geo-Information, 13 (2024), <https://doi.org/10.3390/ijgi13100346>.
- [20] D. KNUTH, *The Art of Computer Programming, Volume 3: Sorting and Searching*, Addison-Wesley, 2nd ed., 1998.
- [21] R. K. V. KOTHURI, S. RAVADA, AND D. ABUGOV, *Quadtree and r-tree indexes in oracle spatial: a comparison using gis data*, in ACM International Conference on Management of Data (SIGMOD), SIGMOD '02, New York, NY, USA, 2002, Association for Computing Machinery, p. 546–557, <https://doi.org/10.1145/564691.564755>.
- [22] H. KRIEGEL AND M. SCHIWETZ, *Performance comparison of point and spatial access methods*, in Design and Implementation of Large Spatial Databases, First Symposium SSD'89, Santa Barbara, California, USA, July 17/18, 1989, Proceedings, vol. 409 of Lecture Notes in Computer Science, Springer, 1989, pp. 89–114, https://doi.org/10.1007/3-540-52208-5_23, https://doi.org/10.1007/3-540-52208-5_23.
- [23] T. LEWINER, V. MELLO, A. PEIXOTO, S. PESCO, AND H. LOPES, *Fast generation of pointerless octree duals*, Computer Graphics Forum, 29 (2010), pp. 1661–1669, <https://doi.org/10.1111/j.1467-8659.2010.01775.x>.
- [24] N. MORRICAL AND J. EDWARDS, *Parallel quadtree construction on collections of objects*, Computers and Graphics, 66 (2017), pp. 162–168, <https://doi.org/https://doi.org/10.1016/j.cag.2017.05.024>. Shape Modeling International 2017.
- [25] M. H. OVERMARS, *The Design of Dynamic Data Structures*, vol. 156 of Lecture Notes in Computer Science, Springer, 1983, <https://doi.org/10.1007/BFb0014927>, <https://doi.org/10.1007/BFb0014927>.
- [26] J. QI, Y. TAO, Y. CHANG, AND R. ZHANG, *Packing r-trees with space-filling curves: Theoretical optimality, empirical efficiency, and bulk-loading parallelizability*, ACM Trans. Database Syst., 45 (2020), pp. 14:1–14:47, <https://doi.org/10.1145/3397506>, <https://doi.org/10.1145/3397506>.
- [27] K. SUGIURA AND Y. ISHIKAWA, *Z-ordered range refinement for multi-dimensional range queries*, CoRR, abs/2305.12732 (2023), <https://arxiv.org/abs/2305.12732>, <https://doi.org/10.1109/TRO.2006.886840>.
- [28] Y. SUN AND G. BLELLOCH, *Parallel range, segment and rectangle queries with augmented maps*, in Proceedings of the Workshop on Algorithm Engineering and Experiments (ALENEX), SIAM, 2019, pp. 159–173, <https://doi.org/10.1137/1.9781611975499.13>.
- [29] H. SUNDAR, R. S. SAMPATH, AND G. BIROS, *Bottom-up construction and 2:1 balance refinement of linear octrees in parallel*, SIAM Journal on Scientific Computing, 30 (2008), pp. 2675–2708, <https://doi.org/10.1137/070681727>.
- [30] S. Y. TANG, Z. HONG, AND Z. XIAOHU, *Linear quadtree encoding of raster data and its spatial analysis approaches*, in Proceedings of the International Cartographic Association Conference (ICC 2001), ICA Commission on Spatial Data Handling, 2001, https://icaci.org/files/documents/ICC_proceedings/ICC2001/icc2001/file/f11020.pdf.
- [31] H. S. TROPF AND H. HERZOG, *Multidimensional range search in dynamically balanced trees*, in Proceedings of the International Conference on Database Theory (ICDT), Amsterdam, The Netherlands, 1981, North-Holland Publishing Co., pp. 153–163.
- [32] I. VAN DER HOOG, L. OST, E. ROTENBERG, AND D. RUTSCHMANN, *Efficient Greedy Discrete Subtrajectory Clustering*, in International Symposium on Computational Geometry (SoCG), O. Aichholzer and H. Wang, eds., vol. 332 of Leibniz International Proceedings in Informatics (LIPIcs), Dagstuhl, Germany, 2025, Schloss Dagstuhl – Leibniz-Zentrum für Informatik, pp. 78:1–78:20, <https://doi.org/10.4230/LIPIcs.SoCG.2025.78>.
- [33] Y. WANG, R. YESANTHARAO, S. YU, L. DHULIPALA, Y. GU, AND J. SHUN, *ParGeo: A library for parallel computational geometry*, in Proceedings of the 30th Annual European Symposium on Algorithms (ESA), Leibniz International Proceedings in Informatics (LIPIcs), Vol.244, Schloss Dagstuhl – Leibniz-Zentrum für Informatik, 2022, pp. 88:1–88:19, <https://doi.org/10.4230/LIPIcs.ESA.2022.88>.
- [34] A. YERSHOVA AND S. LAVALLE, *Improving motion-planning algorithms by efficient nearest-neighbor searching*, Robotics, IEEE Transactions on, 23 (2007), pp. 151 – 157, <https://doi.org/10.1109/TRO.2006.886840>.

- [35] C. ZHANG, Y. ZHANG, W. ZHANG, AND X. LIN, *Inverted linear quadtree: Efficient top-k spatial keyword search*, in Proceedings of the 29th IEEE International Conference on Data Engineering (ICDE), IEEE, 2013, pp. 1706–1717, <https://doi.org/10.1109/ICDE.2013.6544884>.
- [36] J. ZHANG AND L. GRUENWALD, *Efficient quadtree construction for indexing large-scale point data on gpus: Bottom-up vs. top-down*, in Proceedings of the 10th International Workshop on Accelerating Analytics and Data Management Systems (ADMS'19), Los Angeles, CA, USA, 2019, ACM, p. –, https://www.adms-conf.org/2019-camera-ready/zhang_adms19.pdf. Indexing 170M points on GPU with Morton-based quadtree construction.

A Experiments on real-world data.

A.1 The Tiger data. We first consider the performance of our six considered data structures on the **Tiger** and **TigerEast** data sets. These sets contain 35,904,948 and 17,468,291 points respectively. They are, to our knowledge, the only two real-world data sets that are previously used for benchmarking range queries. The **Tiger** data are scattered points across the USA with many empty areas. Our distance queries (q, δ) are generated with random centres q . As a result, we get many empty distance queries.

Construction time. Figure A.1 shows the construction times on **Tiger** and **TigerEast** data sets. **CGAL-R** times out after 10 seconds and **CGAL-KD** uses lazy initialisation and therefore has no construction time. We see that the **Curve-Z** method offers the fastest static construction times and that the gap in performance increases as the size of the data sets increases. We note that this is a non-optimised version of our method that does not make use of dynamic sorting or dynamic Morton encodings. In contrast **Curve-H** is marginally slower than the *R*-trees from Boost. This is primarily because we spend a considerable amount of time computing the ranking of a point along the Hilbert curve. We argue that in all cases, the construction times are competitive.

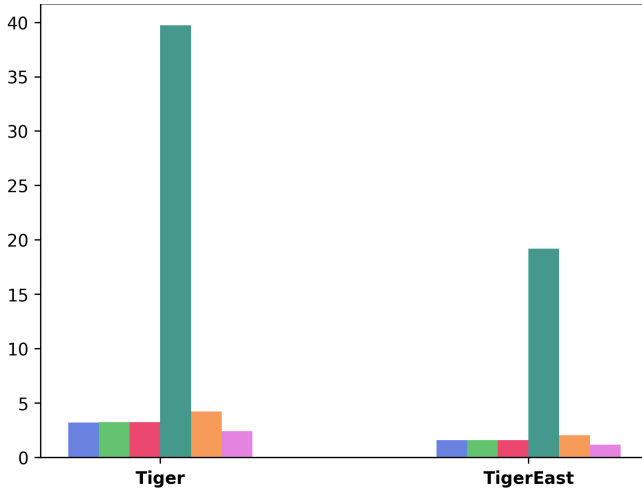


Figure A.1: Construction times (s) of the Boost data structures (Blue/Green/Red) and our **Curve** methods (Orange = **Curve-H**, and Pink = **Curve-Z**), and **PAM-R** (Teal)

Query time. On this data, we see interesting trends for queries (Figure A.2). The Boost queries implementations are *extremely* fast (<0.00005 ms/query, a factor 3.67-37.12 faster than **Curve-Z**). This is especially true for **Gaussian** queries because the centre of the data set is surrounded by empty space, which leads to many empty queries. *R*-trees have a built-in mechanism to

terminate early on empty queries and queries thus terminate after a small constant number of instructions. **CGAL-KD** also shows some interesting trends. The data structure uses a lazy initialisation and therefore spends time building the data structure during queries. This paradigm makes the method competitive on smaller input sizes. As input size grows, the method gradually becomes less competitive (as will be shown in our synthetic experiments). For the **Curve** methods, the **Curve-Z** method offers the fastest runtime of the two because Hilbert curves are slow to evaluate. With 0.00020 ms/query when $n = 40M$, we argue that our queries are still very fast, the Boost implementations (and to a lesser degree **CGAL-KD**) are simply highly optimised.

We may conclude that the *R*-tree implementations are preferable in settings where there are many empty queries. **CGAL-R** and **PAM-R** are not really competitive in this setting whilst **CGAL-KD** performs surprisingly well. Whilst our data is real-world data, we do note that our queries are currently randomly synthetically generated. We do not know whether the query pattern is also realistic but we do believe that these experiments highlight an interesting extremal outcome.

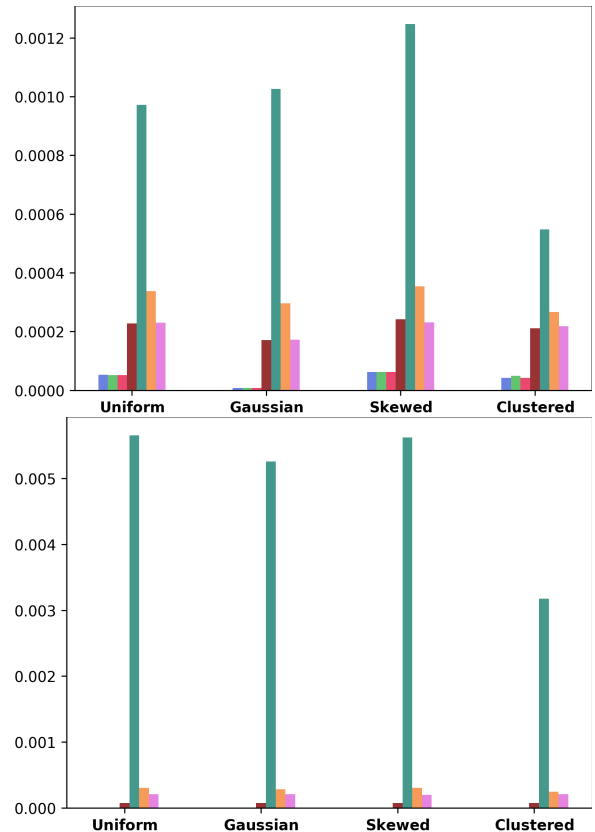


Figure A.2: Query times (ms) times of Boost (Blue/Green/Red), **CGAL-KD** (brown), **Curve-H** (orange), **Curve-Z** (pink) and **PAM-R** (teal).

A.2 Subtrajectory clustering. Van der Hoog et al. [32] present a subtrajectory clustering algorithm. This algorithm constructs for any set of T trajectories with n vertices a distance querying data structure. It then computes a clustering of the trajectories, issuing n distance queries in the process. The time spent on these two types of instructions dominate its running time, and we argue that they therefore greatly benefit from an efficient distance querying data structure. We convert their clustering method into a benchmark for our distance query data structures. In particular, we print the input for their data structure and distance queries. This induces a point collection P and a set of queries Q . We use these in a benchmark, where we first construct the data structure on P and then perform all queries in Q . Our experiments provide a total runtime that measures both the construction time and the total query time over the n queries in Q .

Data sets. We generate the benchmark from [32] by running their algorithm on three real-world data sets: the **Athens-small**, **Berlin**, and **Chicago** data sets from mapconstruction.org. These have respectively 2,840, 192,223, and 118,360 points. We note that [32] sub-sample the **Berlin** and **Chicago** by a factor 10 and 4, respectively. For completeness, we also include the subsampled versions. Finally, the paper in [32] also include synthetic benchmarks. These synthetic benchmarks are less relevant for this paper, since we do extensive experimental evaluation on synthetic data. However, for the sake of completeness, we also include the synthetic data here.

Finally, we note that the algorithm from [32] includes two parameters: m and Δ . We simply supply the algorithms with the parameters that the benchmark in [32] has set.

Results. Figure A.3 shows results on the benchmark derived from [32] on the real-world trajectory data sets. The full table of results can be found in Appendix D.2. Figure A.4 shows the results on the synthetic data that [32] provides in their test suite. These results cannot be found in the appendix, but rather in a zip-file in our repository.

In terms of performance, all three Boost libraries are near identical and are consistently the fastest. In contrast, the range trees **CGAL-R** and **PAM-R** are significantly slower. This is in line with expectations: Range trees are pointer-based and store their leaves in a non-consecutive manner. Both data structures are significantly bottlenecked by pointer traversals and I/O's. **CGAL-KD** remains competitive for smaller datasets but fails to scale as well as other techniques. Finally we note that the **Curve** methods perform reasonably well on this data: they are between $1.19\times$ and $2.4\times$ slower than

Boost, with the performance gap decreasing as dataset size increases. We note that these data sets are relatively small, with only **Berlin** and **Chicago** having moderate size.

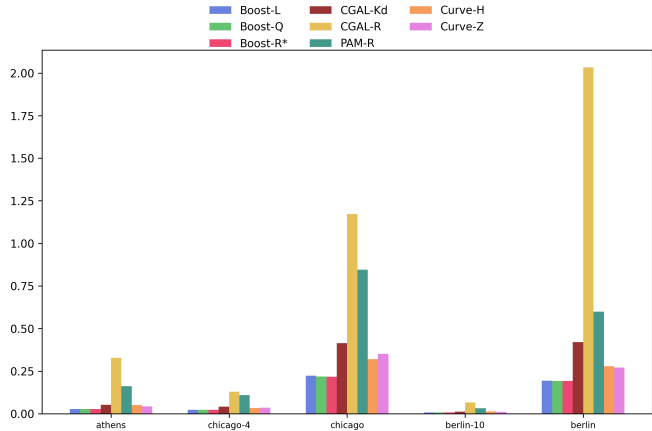


Figure A.3: The runtime (s) of the subtrajectory clustering benchmark on real-world data.

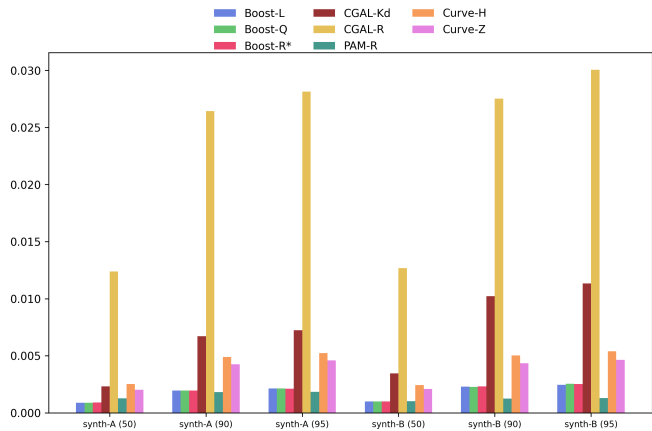


Figure A.4: The runtime (s) of the subtrajectory clustering benchmark on the synthetic data from [32].

B Experiments on static data structures.

We consider the performance of our eight considered data structures on our synthetic data sets. Recall that our experiments fix a bounding box of diameter $\Delta = 2^{16}$. In this bounding box, we generate data from either a **Uniform**, **Gaussian**, **Skewed** or **Clustered** distribution. Queries are then generated as squares with a diameter equal to $\rho\Delta$ with $\rho \in \{0.001, 0.01, 0.02\}$. Finally, the query centres are sampled from either a **Uniform**, **Gaussian**, **Skewed** or **Clustered** distribution. For each fixed set of parameters, we consider construction time and query latency for varying n . This leads to a collection of 384 experiments. The full set of data can be found in our repository. We observe that **CGAL-KD**, **CGAL-R** and **PAM-R** are considerably slower. They are therefore excluded from the discussion but we include them in Appendix D.3.

B.1 Construction time. The construction times of our data structures are independent of the query distribution and shown in Figures B.1, B.3, B.2, and B.4. **CGAL-R** and **PAM-R** are significantly slower, and are therefore excluded from the plots and the further discussion. The relative performance gap between solutions varies marginally.

First we wish to note that the static construction times of both Boost and the Curve methods are *very* fast: near-matching the time it takes to sort the point set by x or y -coordinate. By comparison, **CGAL-R** and **PAM-R** are both more than a factor 50 slower than these implementations. The Boost structures and Curve methods also appear to have roughly the same scaling performance. The Curve-Z data structure is a bit of an outlier in performance. The gap appears to widen as the input size grows and at the largest input size ($n = 40\text{M}$), Curve-Z is a factor 1.46-1.73 faster than Boost.

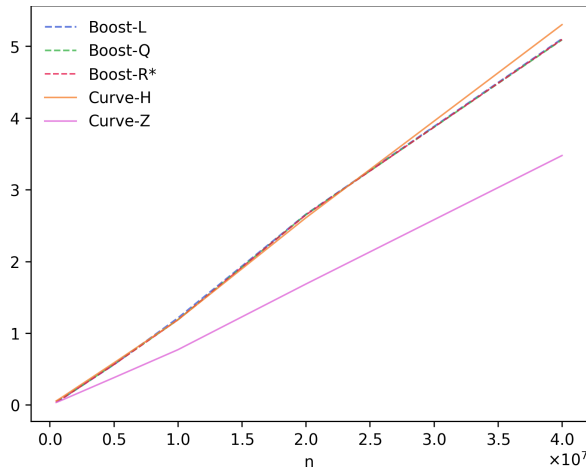


Figure B.1: Construction time (s) on **Uniform** data within a bounding box of $\Delta = 2^{16}$ for increasing input size n .

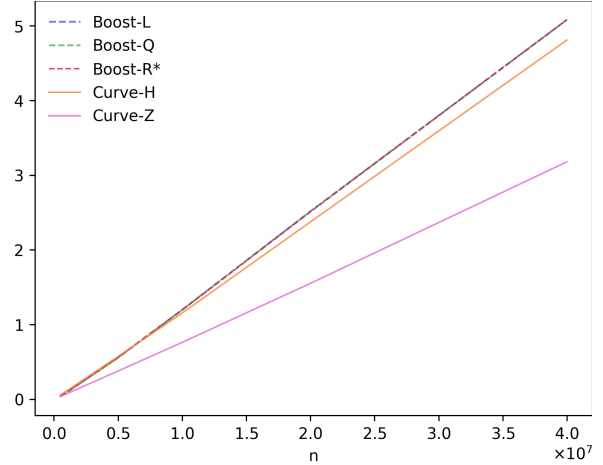


Figure B.2: Construction time (s) on **Skewed** data within a bounding box of $\Delta = 2^{16}$ for increasing input size n .

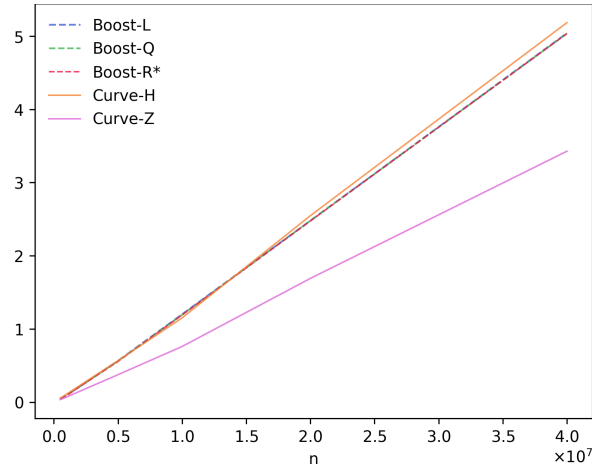


Figure B.3: Construction time (s) on **Gaussian** data within a bounding box of $\Delta = 2^{16}$ for increasing input size n .

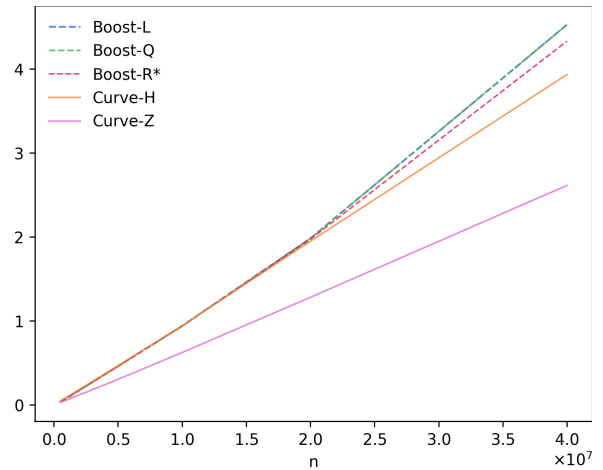


Figure B.4: Construction time (s) on **Clustered** data within a bounding box of $\Delta = 2^{16}$ for increasing input size n .

B.2 Query latency. The data set has only a marginal effect on query performance. In contrast, the query distribution has a significant impact. Figures B.5, B.6, B.7, and B.8 show query latency plots for all four query distributions on **Clustered** data. **CGAL-R** and **PAM-R** are significantly slower, and are therefore excluded from the plots and the further discussion. Perhaps surprisingly, **CGAL-KD** tree is also considerably slower than either **Boost** or our **Curve** methods. Whilst it could be argued that on smaller input, **CGAL-KD** is still relatively competitive we exclude it from the discussion and plots because the gap is considerable for large n .

When query centres are sampled from a **Uniform** distribution, query performance is nearly indistinguishable. The gap is smallest if the input set P is sampled from the **Uniform** distribution and largest if the gap is sampled from the **Clustered** distribution. For **Gaussian** and **Skewed** distributions, performance remains similar. The performance remains within a factor 0.97-2.07 and the median gap is a factor 1.56.

When query centres follow a **Clustered** distribution, the **Boost** implementations are suddenly significantly faster (Figure 5.2 (bottom)). We attribute this performance gain on **Clustered** queries to the **R-tree's** ability to terminate early when queries are empty. If an **R-tree** encounters an empty bounding box near the root, it terminates in constant time. In contrast, our methods based on binary search must fully execute all four binary searches regardless of query outcome. This hypothesis is supported by additional experiments where we enlarge the bounding box, thereby increasing the likelihood that queries return empty results. This hypothesis is also supported by the fact that the gap in performance is largest if the input point set P is sampled from **Clustered** distribution, and the gap is smallest if P is sampled from the **Uniform** distribution.

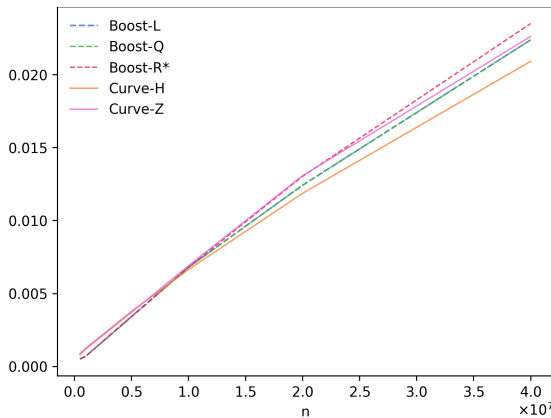


Figure B.5: Query latency (ms) on **Clustered** data within a bounding box of $\Delta = 2^{16}$ for increasing input size n . Queries are generated using a **Uniform** distribution and $\rho = 0.01$.

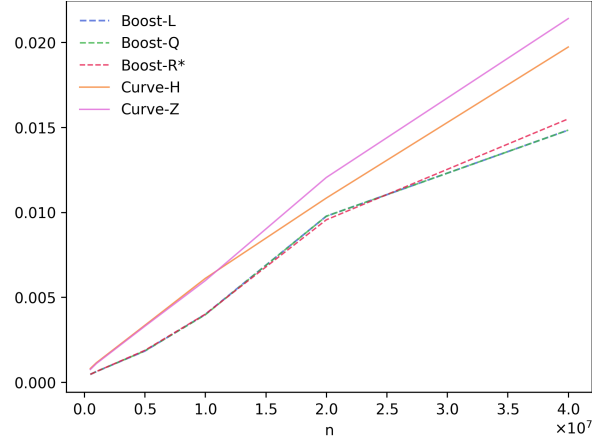


Figure B.6: Query latency (ms) on **Clustered** data within a bounding box of $\Delta = 2^{16}$ for increasing input size n . Queries are generated using a **Gaussian** distribution and $\rho = 0.01$.

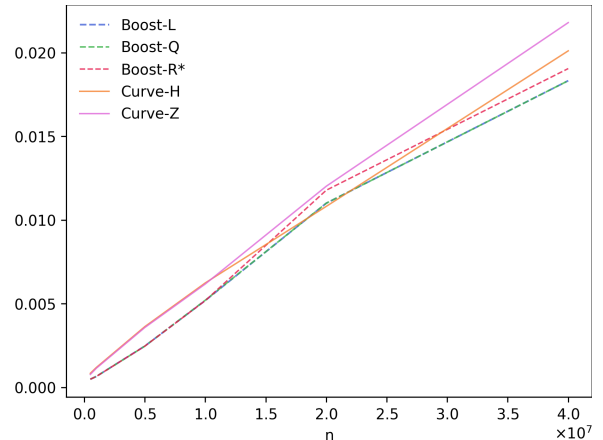


Figure B.7: Query latency (ms) on **Clustered** data within a bounding box of $\Delta = 2^{16}$ for increasing input size n . Queries are generated using a **Skewed** distribution and $\rho = 0.01$.

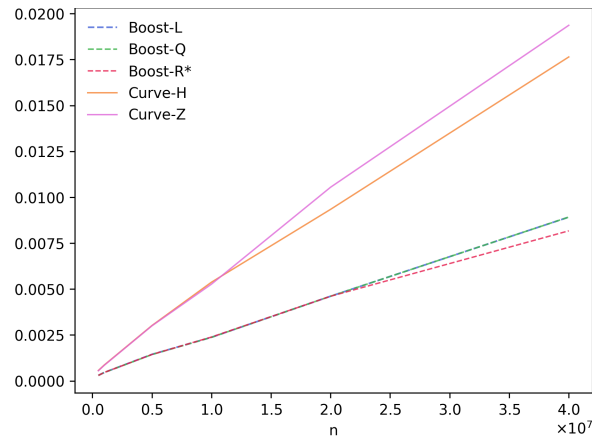


Figure B.8: Query latency (ms) on **Clustered** data within a bounding box of $\Delta = 2^{16}$ for increasing input size n . Queries are generated using a **Clustered** distribution and $\rho = 0.01$.

B.3 Parallel construction. The construction algorithms for **Curve-H** and **Curve-Z** essentially reduce to sorting all points $p \in P$ by $\pi(p)$, where π denotes their position along a Hilbert or Z-curve, respectively. Sorting is trivially parallelisable, and our repository includes a construction algorithm that leverages parallel sorting. Accordingly, we include construction plots for this parallelised case as well. We acknowledge that this comparison is not entirely fair, since we did not explore parallelisation strategies for *R*-tree construction. However, the primary purpose of these plots is to illustrate that our technique is very simple and thereby very simple to parallelise.

As expected, the performance gap in construction times between **Curve-H** and **Curve-Z**, and any Boost implementation, increases significantly under parallelisation. It also remains the case that **Curve-Z** is considerably faster than **Curve-H**.

If one wishes to fully consider parallelised performance, it is worth noting that for any point $p \in \mathbb{Z}^2$, the value $\pi(p)$ can itself be computed in a parallelisable fashion when π is the Z-curve rank. Indeed, the Z-curve rank of a point is simply the bitwise interleaving of its coordinates (see Algorithm 2.2), a computation that can be performed independently for each coordinate. This is not the case for Hilbert curves π' , as the i th bit of $\pi'(p)$ depends on all preceding bits. Consequently, in a highly optimised parallelised implementation, we expect the performance gap to widen further in favour of **Curve-Z**.

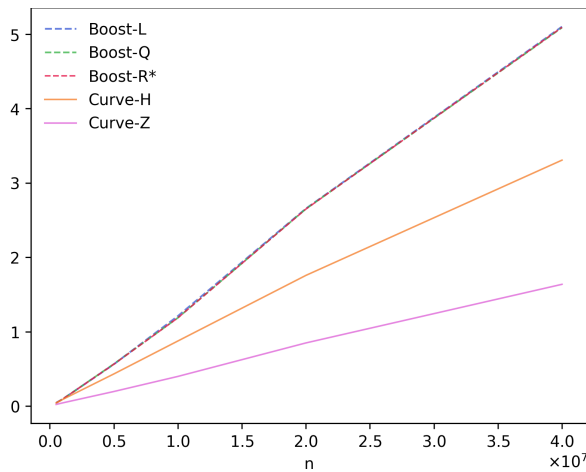


Figure B.9: Construction time (s) on **Uniform** data within a bounding box of $\Delta = 2^{16}$ using parallel sorting.

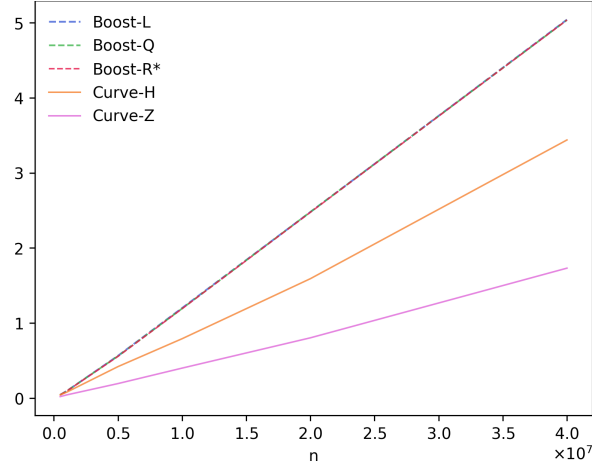


Figure B.10: Construction time (s) on **Gaussian** data within a bounding box of $\Delta = 2^{16}$ using parallel sorting.

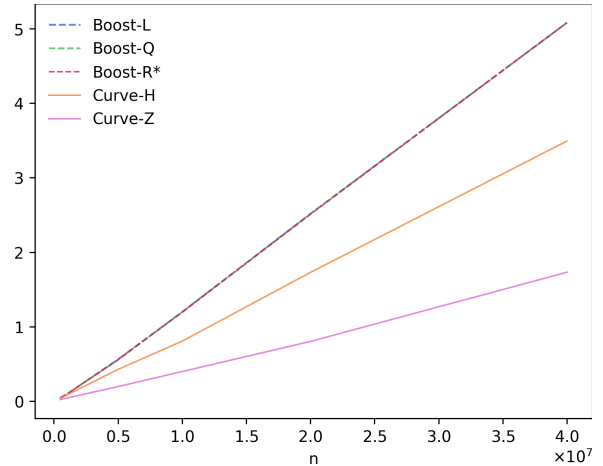


Figure B.11: Construction time (s) on **Skewed** data within a bounding box of $\Delta = 2^{16}$ using parallel sorting.

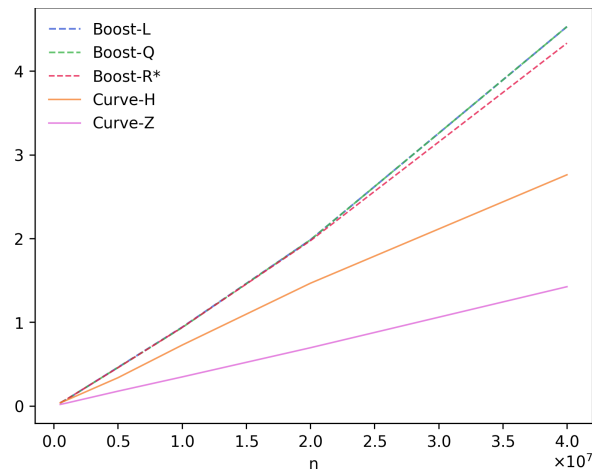


Figure B.12: Construction time (s) on **Clustered** data within a bounding box of $\Delta = 2^{16}$ using parallel sorting.

C Dynamic experiments.

We consider the dynamic performance of our eight data structures. Recall that our experiments fix a bounding box of diameter $\Delta = 2^{16}$. In this bounding box, we generate data from either a **Uniform**, **Gaussian**, **Skewed** or **Clustered** distribution. Queries are then generated as squares with a diameter equal to $\rho\Delta$ with $\rho \in \{0.001, 0.01, 0.02\}$. Finally, the query centres are sampled the four distributions. For each experiment, we consider insertion latency and query latency for the input size $n \in \{0.5M, 1M, 5M, 10M, 20M, 40M\}$. For each fixed n , we first do n insertions and then we measure the query time (Definition 3.1). We note that PAM-R simply times out on small instances. We therefore exclude it from further discussion.

C.1 Insertion latency. Insertion latency measures the average time per insertion in milliseconds. The performance of all data structures is largely independent of the underlying data set. In Figures C.1, C.2, C.3, C.4 we show results for all data sets. Whereas the Boost implementations performed almost identically in static construction tests, they have substantial dynamic performance differences. We conjecture that static R -tree construction relies primarily on sorting P along a space-filling curve (SFC). In dynamic settings, this ordering has less impact, leading to greater variation in performance among Boost implementations. The linear insertion R -tree is notably faster than other variants.

Overall, the **Curve** methods dominate in dynamic insertion performance. As in static construction, the implementation using a **Z-curve** is consistently more efficient than its Hilbert curve counterpart; illustrating that it is easier to compute. The insertion time of **Curve-Z** is between a factor 1.50-13.00 faster than the insertion time of any Boost implementation. The median speedup is a factor 4.5. Notably, the performance gap is relatively independent of the input size.

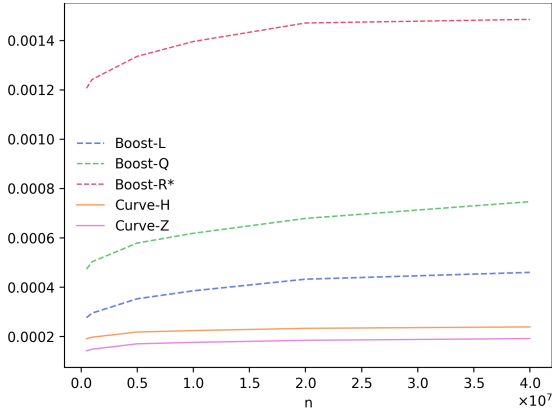


Figure C.1: Insertion time (ms) on **Uniform** data within a bounding box of $\Delta = 2^{16}$ for increasing input size n .

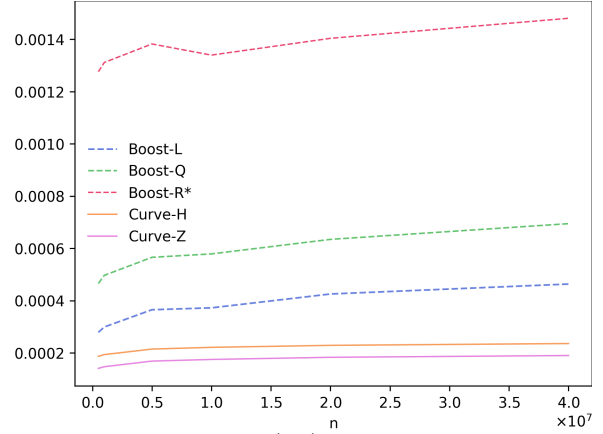


Figure C.2: Insertion time (ms) on **Gaussian** data within a bounding box of $\Delta = 2^{16}$ for increasing input size n .

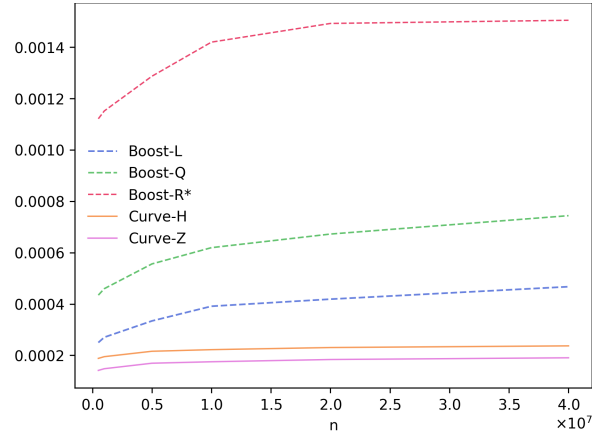


Figure C.3: Insertion time (ms) on **Skewed** data within a bounding box of $\Delta = 2^{16}$ for increasing input size n .

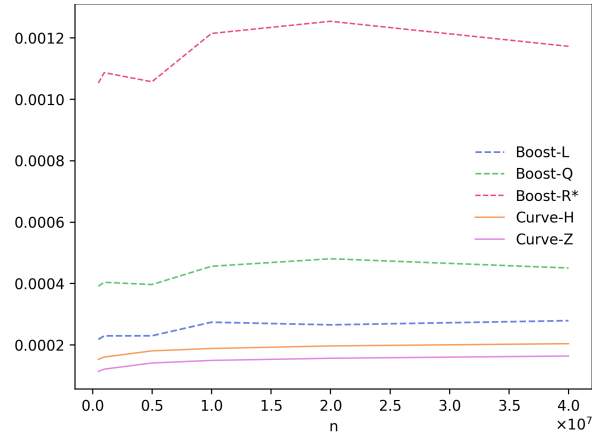


Figure C.4: Insertion time (ms) on **Clustered** data within a bounding box of $\Delta = 2^{16}$ for increasing input size n .

C.2 Queries.

Next, we consider query latency. Recall that our experiments, for each n , first insert n points. We then measure query latency via our latency experiment (see Definition 3.1). The idea of this experiment is that the considered data structures should have less efficient queries in a dynamic setting. Indeed, the bulk construction of R-trees first efficiently groups input points by an ordering along a SFC. In a dynamic setting, the data structures cannot make use of this preprocessing step.

As in the static experiments, the input data set has only a marginal effect on query performance. The query distribution has a reduced impact overall, and results on all distributions except the **Clustered** case follow the same trend. Figures C.5, C.6, C.7 and C.8 illustrate query latency for input from the **Skewed** distribution.

The Boost implementations exhibit significant differences in performance. As expected, **Boost-R*** is the most efficient among them, while **Boost-L** is the least efficient. The various R-tree implementations thereby offer a trade-off between insertion and query efficiency. In contrast to the static setting, the **Curve** methods achieve faster queries than Boost on almost all data sets and query distributions. They consistently provide the best performance, with the median performance being a factor 2.10 faster, except when queries follow a **Clustered** distribution. In this case, **Boost-R*** performs best overall, though the **Curve** methods still outperform the other Boost variants. We observe that **Boost-Q** appears to scale slightly better than any **Curve** method.

When considering both queries and insertions, our proposed method clearly offers the most efficient solution. Although **Boost-R*** achieves better query performance on clustered query workloads, this advantage is offset by its substantially higher insertion cost.

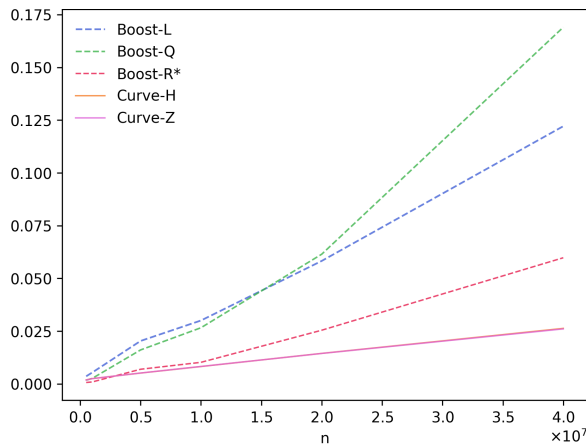


Figure C.5: Query latency (ms) on **Skewed** data within a bounding box of $\Delta = 2^{16}$ for increasing input size n . Queries are generated using a **Uniform** distribution and $\rho = 0.01$.

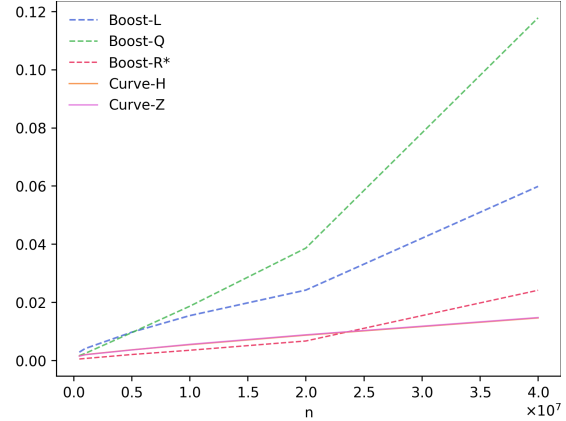


Figure C.6: Query latency (ms) on **Skewed** data within a bounding box of $\Delta = 2^{16}$ for increasing input size n . Queries are generated using a **Gaussian** distribution and $\rho = 0.01$.

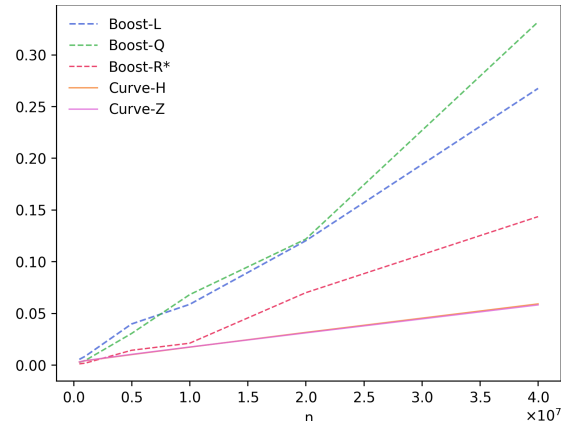


Figure C.7: Query latency (ms) on **Skewed** data within a bounding box of $\Delta = 2^{16}$ for increasing input size n . Queries are generated using a **Skewed** distribution and $\rho = 0.01$.

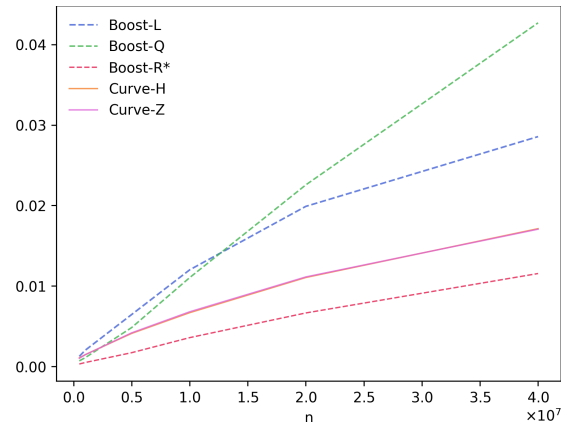


Figure C.8: Query latency (ms) on **Skewed** data within a bounding box of $\Delta = 2^{16}$ for increasing input size n . Queries are generated using a **Clustered** distribution and $\rho = 0.01$.

D Raw data.

D.1 Raw data for real-world experiments.

D.1.1 Construction time Construction time of the data structures on real-world data sets.

	Boost-L	Boost-Q	Boost-R*	PAM-R	Curve-H	Curve-Z
Tiger	3.2020	3.2211	3.2152	39.7284	4.2023	2.4034
TigerEast	1.5847	1.5797	1.5754	19.1869	2.0196	1.1631

Table D.1: Construction time (in seconds) on real-world data.

D.1.2 Query latency Query latency of the data structures on real-world data sets.

	Boost-L	Boost-Q	Boost-R*	CGAL-Kd	PAM-R	Curve-H	Curve-Z
Uniform	0.000052	0.000052	0.000052	0.000227	0.000971	0.000337	0.000230
Gaussian	0.000008	0.000008	0.000008	0.000172	0.001026	0.000297	0.000172
Skewed	0.000063	0.000063	0.000063	0.000242	0.001247	0.000355	0.000231
Clustered	0.000042	0.000050	0.000042	0.000211	0.000547	0.000266	0.000219

Table D.2: Query latency (in milliseconds) on **Tiger** data set where queries are generated using the given distribution and query size $\rho = 0.01$.

	Boost-L	Boost-Q	Boost-R*	CGAL-Kd	PAM-R	Curve-H	Curve-Z
Uniform	0.000005	0.000005	0.000005	0.000075	0.005657	0.000304	0.000209
Gaussian	0.000005	0.000005	0.000005	0.000077	0.005260	0.000283	0.000208
Skewed	0.000005	0.000006	0.000005	0.000076	0.005625	0.000304	0.000196
Clustered	0.000004	0.000004	0.000004	0.000075	0.003174	0.000244	0.000208

Table D.3: Query latency (in milliseconds) on **TigerEast** data set where queries are generated using the given distribution and query size $\rho = 0.01$.

D.2 Raw data for subtrajectory clustering.

Running times of the subtrajectory clustering benchmark for real-world data sets.

Δ	Boost-L	Boost-Q	Boost-R*	CGAL-Kd	CGAL-R	PAM-R	Curve-H	Curve-Z
50	0.022	0.022	0.022	0.042	0.300	0.133	0.049	0.039
100	0.027	0.027	0.027	0.051	0.328	0.162	0.051	0.043
200	0.035	0.035	0.035	0.068	0.372	0.210	0.060	0.055

Table D.4: Running time (in seconds) of the clustering benchmark on athens data set.

Δ	Boost-L	Boost-Q	Boost-R*	CGAL-Kd	CGAL-R	PAM-R	Curve-H	Curve-Z
50	0.005	0.006	0.006	0.009	0.060	0.025	0.012	0.009
100	0.007	0.007	0.007	0.012	0.066	0.032	0.013	0.011
200	0.009	0.009	0.009	0.017	0.083	0.043	0.016	0.015

Table D.5: Running time (in seconds) of the clustering benchmark on berlin-10 data set.

Δ	Boost-L	Boost-Q	Boost-R*	CGAL-Kd	CGAL-R	PAM-R	Curve-H	Curve-Z
50	0.132	0.131	0.132	0.271	1.527	0.448	0.199	0.179
100	0.193	0.192	0.192	0.420	2.033	0.600	0.278	0.270
200	0.334	0.332	0.333	0.746	3.145	0.942	0.495	0.516

Table D.6: Running time (in seconds) of the clustering benchmark on berlin data set.

Δ	Boost-L	Boost-Q	Boost-R*	CGAL-Kd	CGAL-R	PAM-R	Curve-H	Curve-Z
50	0.018	0.018	0.018	0.029	0.113	0.080	0.025	0.025
100	0.023	0.023	0.023	0.041	0.130	0.109	0.034	0.035
200	0.033	0.033	0.033	0.067	0.158	0.162	0.060	0.064

Table D.7: Running time (in seconds) of the clustering benchmark on chicago-4 data set.

Δ	Boost-L	Boost-Q	Boost-R*	CGAL-Kd	CGAL-R	PAM-R	Curve-H	Curve-Z
50	0.152	0.152	0.154	0.260	0.895	0.563	0.184	0.201
100	0.223	0.218	0.216	0.414	1.172	0.846	0.320	0.351
200	0.368	0.372	0.369	0.746	1.731	1.407	0.704	0.748

Table D.8: Running time (in seconds) of the clustering benchmark on chicago data set.

D.3 Raw data for the static experiments.

D.3.1 Construction time Construction time of the data structures on synthetic data sets for increasing n . Recall that CGAL-KD does a lazy initialisation.

n	Boost-L	Boost-Q	Boost-R*	CGAL-Kd	CGAL-R	PAM-R	Curve-H	Curve-Z
$5 \cdot 10^5$	0.0437	0.0432	0.0434	-	1.2561	0.4921	0.0557	0.0350
$10 \cdot 10^5$	0.0928	0.0922	0.0926	-	2.8403	1.0098	0.1123	0.0712
$50 \cdot 10^5$	0.5617	0.5653	0.5619	-	17.8072	5.0076	0.5851	0.3796
$100 \cdot 10^5$	1.2097	1.1865	1.1861	-	38.6311	9.7230	1.1853	0.7692
$200 \cdot 10^5$	2.6552	2.6515	2.6488	-	-	18.7414	2.6082	1.6852
$400 \cdot 10^5$	5.1020	5.0890	5.0936	-	-	35.7933	5.2996	3.4760

Table D.9: Construction time (in seconds) on **Uniform** data within a bounding box of $\Delta = 2^{16}$ for increasing input size n .

n	Boost-L	Boost-Q	Boost-R*	CGAL-Kd	CGAL-R	PAM-R	Curve-H	Curve-Z
$5 \cdot 10^5$	0.0444	0.0452	0.0442	-	1.2757	0.4807	0.0542	0.0347
$10 \cdot 10^5$	0.0936	0.0938	0.0929	-	2.8418	0.9582	0.1101	0.0706
$50 \cdot 10^5$	0.5640	0.5604	0.5557	-	17.7692	4.5432	0.5657	0.3748
$100 \cdot 10^5$	1.2000	1.1938	1.1913	-	38.2545	8.7445	1.1514	0.7602
$200 \cdot 10^5$	2.4791	2.4798	2.4753	-	-	16.6868	2.5480	1.6910
$400 \cdot 10^5$	5.0419	5.0367	5.0365	-	-	31.4256	5.1857	3.4287

Table D.10: Construction time (in seconds) on **Gaussian** data within a bounding box of $\Delta = 2^{16}$ for increasing input size n .

n	Boost-L	Boost-Q	Boost-R*	CGAL-Kd	CGAL-R	PAM-R	Curve-H	Curve-Z
$5 \cdot 10^5$	0.0442	0.0444	0.0441	-	1.2651	0.4840	0.0547	0.0349
$10 \cdot 10^5$	0.0912	0.0919	0.0923	-	2.8736	0.9802	0.1106	0.0719
$50 \cdot 10^5$	0.5594	0.5529	0.5568	-	17.7780	4.7335	0.5700	0.3767
$100 \cdot 10^5$	1.1968	1.1961	1.1926	-	38.2665	9.1526	1.1529	0.7601
$200 \cdot 10^5$	2.5149	2.5149	2.5081	-	-	17.5535	2.3735	1.5508
$400 \cdot 10^5$	5.0809	5.0812	5.0822	-	-	31.8056	4.8094	3.1791

Table D.11: Construction time (in seconds) on **Skewed** data within a bounding box of $\Delta = 2^{16}$ for increasing input size n .

n	Boost-L	Boost-Q	Boost-R*	CGAL-Kd	CGAL-R	PAM-R	Curve-H	Curve-Z
$5 \cdot 10^5$	0.0370	0.0373	0.0373	-	1.1843	0.4497	0.0445	0.0282
$10 \cdot 10^5$	0.0781	0.0791	0.0804	-	2.7906	0.9359	0.0897	0.0571
$50 \cdot 10^5$	0.4610	0.4595	0.4571	-	16.0696	4.7058	0.4665	0.3033
$100 \cdot 10^5$	0.9399	0.9359	0.9383	-	33.8600	9.1630	0.9422	0.6232
$200 \cdot 10^5$	1.9831	1.9831	1.9730	-	-	17.6591	1.9495	1.2808
$400 \cdot 10^5$	4.5295	4.5295	4.3323	-	-	33.8092	3.9352	2.6141

Table D.12: Construction time (in seconds) on **Clustered** data within a bounding box of $\Delta = 2^{16}$ for increasing input size n .

D.3.2 Query latency Query latency of the data structures on synthetic data sets for increasing n .

n	Boost-L	Boost-Q	Boost-R*	CGAL-Kd	CGAL-R	PAM-R	Curve-H	Curve-Z
$5 \cdot 10^5$	0.5123	0.5130	0.5129	1.4296	13.8282	5.7570	0.9116	0.8548
$10 \cdot 10^5$	0.6952	0.6949	0.6937	4.7010	20.2008	9.3211	1.2898	1.2395
$50 \cdot 10^5$	3.4598	3.4666	3.4557	23.0262	48.1900	25.3053	3.8243	3.7860
$100 \cdot 10^5$	6.8695	6.8657	6.8694	43.8799	74.3207	39.2369	7.0752	6.9672
$200 \cdot 10^5$	12.1488	13.1272	12.4408	85.1912	-	62.8014	11.4833	12.6693
$400 \cdot 10^5$	23.7910	23.5568	23.4765	182.4548	-	108.6335	21.7595	23.3657

Table D.13: Query latency (milliseconds per query) on **Uniform** data within a bounding box of $\Delta = 2^{16}$ for increasing input size n . Queries are generated using a **Uniform** distribution and query size $\rho = 0.01$.

n	Boost-L	Boost-Q	Boost-R*	CGAL-Kd	CGAL-R	PAM-R	Curve-H	Curve-Z
$5 \cdot 10^5$	0.4188	0.4186	0.4199	0.9935	9.3203	3.6061	0.7373	0.6592
$10 \cdot 10^5$	0.5937	0.5946	0.5933	3.5028	14.3402	6.0859	1.0518	0.9736
$50 \cdot 10^5$	2.9819	2.9882	2.9883	20.0066	40.7696	18.7371	3.1670	3.0278
$100 \cdot 10^5$	6.0027	6.0206	5.9866	40.7345	67.5042	32.9752	5.8278	5.5590
$200 \cdot 10^5$	11.5205	11.4012	11.4632	84.7235	-	59.7721	10.4938	11.1149
$400 \cdot 10^5$	20.5152	20.6652	21.6063	182.9277	-	121.4643	20.2153	20.9961

Table D.14: Query latency (milliseconds per query) on **Gaussian** data within a bounding box of $\Delta = 2^{16}$ for increasing input size n . Queries are generated using a **Uniform** distribution and query size $\rho = 0.01$.

n	Boost-L	Boost-Q	Boost-R*	CGAL-Kd	CGAL-R	PAM-R	Curve-H	Curve-Z
$5 \cdot 10^5$	0.4811	0.4804	0.4813	1.2432	12.5732	4.8447	0.9018	0.7490
$10 \cdot 10^5$	0.6622	0.6596	0.6595	4.0319	18.6361	8.1395	1.1708	1.1045
$50 \cdot 10^5$	3.2371	3.2265	3.2273	20.9583	46.1370	22.3922	3.4113	3.3009
$100 \cdot 10^5$	6.3248	6.3702	6.3215	41.8941	73.5391	35.8342	6.2717	6.0584
$200 \cdot 10^5$	11.9340	12.2196	12.2259	84.9726	-	60.9444	10.7955	11.5797
$400 \cdot 10^5$	21.5020	21.5733	21.4835	175.8972	-	114.8584	19.4802	20.6932

Table D.15: Query latency (milliseconds per query) on **Skewed** data within a bounding box of $\Delta = 2^{16}$ for increasing input size n . Queries are generated using a **Uniform** distribution and query size $\rho = 0.01$.

n	Boost-L	Boost-Q	Boost-R*	CGAL-Kd	CGAL-R	PAM-R	Curve-H	Curve-Z
$5 \cdot 10^5$	0.4977	0.4984	0.4972	1.1727	13.5316	6.7720	0.8633	0.7930
$10 \cdot 10^5$	0.6850	0.6843	0.6849	3.6039	19.7710	10.3029	1.2287	1.1775
$50 \cdot 10^5$	3.4089	3.3654	3.3941	16.6843	47.2722	25.8491	3.7610	3.6905
$100 \cdot 10^5$	6.7859	6.7826	6.7821	30.0631	72.5974	39.7537	6.6250	6.8892
$200 \cdot 10^5$	12.4090	12.4090	13.0199	55.6672	-	64.5132	11.8561	13.0684
$400 \cdot 10^5$	22.3856	22.3856	23.5062	106.7329	-	109.8738	20.9155	22.6177

Table D.16: Query latency (milliseconds per query) on **Clustered** data within a bounding box of $\Delta = 2^{16}$ for increasing input size n . Queries are generated using a **Uniform** distribution and query size $\rho = 0.01$.

n	Boost-L	Boost-Q	Boost-R*	CGAL-Kd	CGAL-R	PAM-R	Curve-H	Curve-Z
$5 \cdot 10^5$	0.4761	0.4769	0.4776	1.1535	11.8006	5.1324	0.8547	0.8073
$10 \cdot 10^5$	0.6572	0.6555	0.6554	2.4103	17.4689	6.4362	1.2423	1.1913
$50 \cdot 10^5$	1.9432	1.9297	1.9343	18.9147	44.6873	20.1761	3.5206	3.4688
$100 \cdot 10^5$	3.9448	3.9390	3.9346	40.2557	71.1384	33.5906	6.0681	5.9265
$200 \cdot 10^5$	6.5098	6.5661	9.2925	70.3091	-	56.5592	11.0977	12.2861
$400 \cdot 10^5$	20.1372	20.1365	20.0727	177.3113	-	103.8655	20.0416	22.2329

Table D.17: Query latency (milliseconds per query) on **Uniform** data within a bounding box of $\Delta = 2^{16}$ for increasing input size n . Queries are generated using a **Gaussian** distribution and query size $\rho = 0.01$.

n	Boost-L	Boost-Q	Boost-R*	CGAL-Kd	CGAL-R	PAM-R	Curve-H	Curve-Z
$5 \cdot 10^5$	1.1225	1.1238	1.1216	3.3514	24.1058	9.6496	2.1316	2.0908
$10 \cdot 10^5$	1.6834	1.6802	1.6838	13.2294	39.6985	17.1631	3.4784	3.4132
$50 \cdot 10^5$	10.7912	10.6023	10.7566	86.9520	139.3590	62.7699	12.9792	12.4745
$100 \cdot 10^5$	23.8764	24.0311	24.1022	179.7313	250.5544	123.3084	24.9816	23.7542
$200 \cdot 10^5$	49.0798	50.2801	47.8645	401.4790	-	257.4248	48.6464	50.7295
$400 \cdot 10^5$	90.4314	90.9306	91.2600	842.4884	-	581.7437	95.2989	97.8273

Table D.18: Query latency (milliseconds per query) on **Gaussian** data within a bounding box of $\Delta = 2^{16}$ for increasing input size n . Queries are generated using a **Gaussian** distribution and query size $\rho = 0.01$.

n	Boost-L	Boost-Q	Boost-R*	CGAL-Kd	CGAL-R	PAM-R	Curve-H	Curve-Z
$5 \cdot 10^5$	0.3690	0.3708	0.3700	0.7895	8.8872	2.8995	0.6248	0.5617
$10 \cdot 10^5$	0.4690	0.4679	0.4660	1.4614	13.1162	4.4723	0.8478	0.7836
$50 \cdot 10^5$	1.2755	1.2725	1.2683	8.8361	30.9978	12.9556	2.1292	2.0765
$100 \cdot 10^5$	2.1285	2.1234	2.1251	20.4568	46.4909	21.9805	3.4437	3.3768
$200 \cdot 10^5$	4.2327	4.3112	4.2882	44.4763	-	34.0202	5.5155	6.2580
$400 \cdot 10^5$	9.1526	9.4526	9.4944	93.4946	-	57.5924	10.0475	11.1221

Table D.19: Query latency (milliseconds per query) on **Skewed** data within a bounding box of $\Delta = 2^{16}$ for increasing input size n . Queries are generated using a **Gaussian** distribution and query size $\rho = 0.01$.

n	Boost-L	Boost-Q	Boost-R*	CGAL-Kd	CGAL-R	PAM-R	Curve-H	Curve-Z
$5 \cdot 10^5$	0.4599	0.4606	0.4604	0.9557	10.6306	4.8967	0.8054	0.7470
$10 \cdot 10^5$	0.6257	0.6255	0.6254	1.6236	15.8725	7.8563	1.1445	1.0978
$50 \cdot 10^5$	1.8330	1.8407	1.8714	10.8099	41.3551	22.3770	3.3463	3.2917
$100 \cdot 10^5$	3.9900	3.9698	4.0030	26.3586	68.6408	37.2133	6.1095	5.9789
$200 \cdot 10^5$	9.7692	9.7692	9.5566	54.7516	-	63.2143	10.8374	12.0484
$400 \cdot 10^5$	14.8379	14.8379	15.4990	95.8589	-	106.9748	19.7295	21.4037

Table D.20: Query latency (milliseconds per query) on **Clustered** data within a bounding box of $\Delta = 2^{16}$ for increasing input size n . Queries are generated using a **Gaussian** distribution and query size $\rho = 0.01$.

n	Boost-L	Boost-Q	Boost-R*	CGAL-Kd	CGAL-R	PAM-R	Curve-H	Curve-Z
$5 \cdot 10^5$	0.5002	0.5002	0.4993	1.2051	13.0685	4.6224	0.8822	0.8218
$10 \cdot 10^5$	0.6713	0.6703	0.6711	3.2438	18.8782	7.6986	1.2591	1.2121
$50 \cdot 10^5$	2.4120	2.4088	2.4063	21.1801	46.5712	22.6082	3.5784	3.5266
$100 \cdot 10^5$	5.2819	5.2471	5.2852	42.1911	72.5779	36.3158	6.3004	6.2037
$200 \cdot 10^5$	8.7185	8.7267	8.8191	77.2917	-	61.6884	11.1097	12.2802
$400 \cdot 10^5$	22.3146	22.3473	23.0098	177.8053	-	104.4038	20.8084	22.4799

Table D.21: Query latency (milliseconds per query) on **Uniform** data within a bounding box of $\Delta = 2^{16}$ for increasing input size n . Queries are generated using a **Skewed** distribution and query size $\rho = 0.01$.

n	Boost-L	Boost-Q	Boost-R*	CGAL-Kd	CGAL-R	PAM-R	Curve-H	Curve-Z
$5 \cdot 10^5$	0.2852	0.2854	0.2848	0.5999	6.4215	2.3730	0.5110	0.4453
$10 \cdot 10^5$	0.3968	0.3971	0.3966	1.7614	9.7482	3.8684	0.6972	0.6230
$50 \cdot 10^5$	1.5492	1.5490	1.5337	10.5091	26.7876	11.0378	1.8268	1.7319
$100 \cdot 10^5$	3.1684	3.1648	3.1747	21.7913	42.8820	18.5559	3.1786	3.0254
$200 \cdot 10^5$	6.1507	6.1347	6.1463	45.4674	-	33.3537	5.6893	6.0473
$400 \cdot 10^5$	11.3735	10.8917	11.1611	95.7680	-	65.2414	10.6569	11.1679

Table D.22: Query latency (milliseconds per query) on **Gaussian** data within a bounding box of $\Delta = 2^{16}$ for increasing input size n . Queries are generated using a **Skewed** distribution and query size $\rho = 0.01$.

n	Boost-L	Boost-Q	Boost-R*	CGAL-Kd	CGAL-R	PAM-R	Curve-H	Curve-Z
$5 \cdot 10^5$	0.7335	0.7318	0.7336	2.1795	17.2407	7.0425	1.3792	1.3415
$10 \cdot 10^5$	1.1536	1.1536	1.1532	7.7331	26.8350	12.2167	2.1167	2.0761
$50 \cdot 10^5$	6.3242	6.2998	6.2901	45.6982	79.9392	38.7776	7.1825	6.9741
$100 \cdot 10^5$	13.3023	13.3396	13.3392	93.6417	136.8689	67.1204	13.4573	13.0449
$200 \cdot 10^5$	28.0904	28.0863	27.3498	201.2210	-	125.7895	23.7721	25.5024
$400 \cdot 10^5$	45.6965	48.4398	48.3557	413.0832	-	262.6430	44.3314	46.5890

Table D.23: Query latency (milliseconds per query) on **Skewed** data within a bounding box of $\Delta = 2^{16}$ for increasing input size n . Queries are generated using a **Skewed** distribution and query size $\rho = 0.01$.

n	Boost-L	Boost-Q	Boost-R*	CGAL-Kd	CGAL-R	PAM-R	Curve-H	Curve-Z
$5 \cdot 10^5$	0.4845	0.4852	0.4847	1.0118	12.2520	5.7791	0.8400	0.7713
$10 \cdot 10^5$	0.6525	0.6525	0.6525	2.1309	17.8156	8.8406	1.1890	1.1451
$50 \cdot 10^5$	2.4661	2.4603	2.4610	15.3792	46.1612	25.1331	3.6268	3.5748
$100 \cdot 10^5$	5.1890	5.2058	5.1835	28.6282	70.2548	38.1353	6.2415	6.1773
$200 \cdot 10^5$	11.0046	11.0046	11.7802	54.0549	-	61.9821	10.8151	12.0188
$400 \cdot 10^5$	18.3267	18.3267	19.0511	101.3854	-	107.2180	20.1106	21.7973

Table D.24: Query latency (milliseconds per query) on **Clustered** data within a bounding box of $\Delta = 2^{16}$ for increasing input size n . Queries are generated using a **Skewed** distribution and query size $\rho = 0.01$.

n	Boost-L	Boost-Q	Boost-R*	CGAL-Kd	CGAL-R	PAM-R	Curve-H	Curve-Z
$5 \cdot 10^5$	0.3274	0.3279	0.3279	0.8109	3.2999	2.8610	0.6296	0.6065
$10 \cdot 10^5$	0.4929	0.4924	0.4923	1.4198	4.8425	4.2149	0.9721	0.9572
$50 \cdot 10^5$	1.4499	1.4557	1.4505	5.8218	13.4677	10.3348	3.1223	3.0966
$100 \cdot 10^5$	2.6587	2.3849	2.3862	11.4246	24.5397	16.0578	5.5143	5.4064
$200 \cdot 10^5$	4.9988	5.0219	5.0287	24.5018	-	26.1729	10.4330	11.6557
$400 \cdot 10^5$	8.1301	8.1292	8.1245	56.6624	-	44.9861	19.6878	21.3529

Table D.25: Query latency (milliseconds per query) on **Uniform** data within a bounding box of $\Delta = 2^{16}$ for increasing input size n . Queries are generated using a **Clustered** distribution and query size $\rho = 0.01$.

n	Boost-L	Boost-Q	Boost-R*	CGAL-Kd	CGAL-R	PAM-R	Curve-H	Curve-Z
$5 \cdot 10^5$	0.2633	0.2613	0.2633	0.6181	2.0617	1.7510	0.5763	0.5645
$10 \cdot 10^5$	0.4056	0.4056	0.4066	1.1819	2.9099	2.5392	0.8266	0.8117
$50 \cdot 10^5$	1.2701	1.2684	1.2668	5.8572	11.7963	8.4530	3.1007	3.0838
$100 \cdot 10^5$	2.2582	2.2545	2.2595	14.1093	24.5711	14.0890	5.8400	5.6381
$200 \cdot 10^5$	4.4948	4.4193	4.4910	31.4147	-	18.8802	11.6920	12.3859
$400 \cdot 10^5$	8.3048	8.1661	8.2838	67.3464	-	33.3626	22.6037	23.4065

Table D.26: Query latency (milliseconds per query) on **Gaussian** data within a bounding box of $\Delta = 2^{16}$ for increasing input size n . Queries are generated using a **Clustered** distribution and query size $\rho = 0.01$.

n	Boost-L	Boost-Q	Boost-R*	CGAL-Kd	CGAL-R	PAM-R	Curve-H	Curve-Z
$5 \cdot 10^5$	0.2875	0.2876	0.2875	0.6076	2.7276	2.2256	0.5265	0.5037
$10 \cdot 10^5$	0.4263	0.4263	0.4281	1.0830	3.9813	3.1747	0.8372	0.8164
$50 \cdot 10^5$	1.3674	1.3679	1.3673	4.8242	10.9349	8.1083	2.6603	2.6180
$100 \cdot 10^5$	2.2923	2.2920	2.2943	9.8658	21.5774	13.1560	4.6548	4.5488
$200 \cdot 10^5$	4.4803	4.4909	4.4825	21.7318	-	20.0183	8.2309	8.9792
$400 \cdot 10^5$	8.0535	8.0568	8.0196	51.2552	-	32.4622	15.8447	16.8376

Table D.27: Query latency (milliseconds per query) on **Skewed** data within a bounding box of $\Delta = 2^{16}$ for increasing input size n . Queries are generated using a **Clustered** distribution and query size $\rho = 0.01$.

n	Boost-L	Boost-Q	Boost-R*	CGAL-Kd	CGAL-R	PAM-R	Curve-H	Curve-Z
$5 \cdot 10^5$	0.2988	0.2989	0.2987	0.6062	2.8861	2.3345	0.5673	0.5514
$10 \cdot 10^5$	0.4586	0.4581	0.4589	1.0538	4.4377	3.5099	0.8670	0.8508
$50 \cdot 10^5$	1.4441	1.4348	1.4387	3.8622	12.2541	9.5157	3.0158	2.9997
$100 \cdot 10^5$	2.3744	2.3731	2.3881	6.7340	22.5922	14.9881	5.3768	5.2712
$200 \cdot 10^5$	4.6115	4.6115	4.6092	12.4562	-	24.9096	9.3435	10.5489
$400 \cdot 10^5$	8.9207	8.9207	8.1729	25.7658	-	43.5225	17.6439	19.3675

Table D.28: Query latency (milliseconds per query) on **Clustered** data within a bounding box of $\Delta = 2^{16}$ for increasing input size n . Queries are generated using a **Clustered** distribution and query size $\rho = 0.01$.

D.4 Raw data for the dynamic experiments.

D.4.1 Insertion time Insertion time of the data structures on synthetic data sets for increasing n . Recall that CGAL-KD does a lazy initialisation.

n	Boost-L	Boost-Q	Boost-R*	CGAL-Kd	CGAL-R	Curve-H	Curve-Z
$5 \cdot 10^5$	0.0003	0.0005	0.0012	0.0000	0.0027	0.0002	0.0001
$10 \cdot 10^5$	0.0003	0.0005	0.0012	0.0000	0.0029	0.0002	0.0001
$50 \cdot 10^5$	0.0004	0.0006	0.0013	0.0000	0.0037	0.0002	0.0002
$100 \cdot 10^5$	0.0004	0.0006	0.0014	0.0000	0.0038	0.0002	0.0002
$200 \cdot 10^5$	0.0004	0.0007	0.0015	0.0000	-	0.0002	0.0002
$400 \cdot 10^5$	0.0005	0.0007	0.0015	0.0000	-	0.0002	0.0002

Table D.29: Insertion time (in milliseconds) on **Uniform** data within a bounding box of $\Delta = 2^{16}$ for increasing input size n .

n	Boost-L	Boost-Q	Boost-R*	CGAL-Kd	CGAL-R	Curve-H	Curve-Z
$5 \cdot 10^5$	0.0003	0.0005	0.0013	0.0000	0.0026	0.0002	0.0001
$10 \cdot 10^5$	0.0003	0.0005	0.0013	0.0000	0.0029	0.0002	0.0001
$50 \cdot 10^5$	0.0004	0.0006	0.0014	0.0000	0.0037	0.0002	0.0002
$100 \cdot 10^5$	0.0004	0.0006	0.0013	0.0000	0.0038	0.0002	0.0002
$200 \cdot 10^5$	0.0004	0.0006	0.0014	0.0000	-	0.0002	0.0002
$400 \cdot 10^5$	0.0005	0.0007	0.0015	0.0000	-	0.0002	0.0002

Table D.30: Insertion time (in milliseconds) on **Gaussian** data within a bounding box of $\Delta = 2^{16}$ for increasing input size n .

n	Boost-L	Boost-Q	Boost-R*	CGAL-Kd	CGAL-R	Curve-H	Curve-Z
$5 \cdot 10^5$	0.0002	0.0004	0.0011	0.0000	0.0025	0.0002	0.0001
$10 \cdot 10^5$	0.0003	0.0005	0.0012	0.0000	0.0028	0.0002	0.0001
$50 \cdot 10^5$	0.0003	0.0006	0.0013	0.0000	0.0036	0.0002	0.0002
$100 \cdot 10^5$	0.0004	0.0006	0.0014	0.0000	0.0039	0.0002	0.0002
$200 \cdot 10^5$	0.0004	0.0007	0.0015	0.0000	-	0.0002	0.0002
$400 \cdot 10^5$	0.0005	0.0007	0.0015	0.0000	-	0.0002	0.0002

Table D.31: Insertion time (in milliseconds) on **Skewed** data within a bounding box of $\Delta = 2^{16}$ for increasing input size n .

n	Boost-L	Boost-Q	Boost-R*	CGAL-Kd	CGAL-R	Curve-H	Curve-Z
$5 \cdot 10^5$	0.0002	0.0004	0.0011	0.0000	0.0026	0.0002	0.0001
$10 \cdot 10^5$	0.0002	0.0004	0.0011	0.0000	0.0027	0.0002	0.0001
$50 \cdot 10^5$	0.0002	0.0004	0.0011	0.0000	0.0032	0.0002	0.0001
$100 \cdot 10^5$	0.0003	0.0005	0.0012	0.0000	0.0035	0.0002	0.0001
$200 \cdot 10^5$	0.0003	0.0005	0.0013	0.0000	-	0.0002	0.0002
$400 \cdot 10^5$	0.0003	0.0005	0.0012	0.0000	-	0.0002	0.0002

Table D.32: Insertion time (in milliseconds) on **Clustered** data within a bounding box of $\Delta = 2^{16}$ for increasing input size n .

D.4.2 Query latency Query latency of the data structures on synthetic data sets for increasing n .

n	Boost-L	Boost-Q	Boost-R*	CGAL-Kd	CGAL-R	Curve-H	Curve-Z
$5 \cdot 10^5$	4.0801	1.7163	0.8089	1.3040	11.5244	2.1549	2.1396
$10 \cdot 10^5$	6.1201	2.7733	1.1913	2.2615	17.2715	2.8159	2.8853
$50 \cdot 10^5$	19.9088	10.3252	7.4708	22.1473	50.0065	5.6239	5.8225
$100 \cdot 10^5$	39.7134	26.0224	11.4732	40.2002	75.6292	9.2281	9.9327
$200 \cdot 10^5$	72.3092	60.5440	27.4603	80.9999	-	15.6865	15.8866
$400 \cdot 10^5$	140.5460	138.7588	63.7328	168.8687	-	28.3019	28.4297

Table D.33: Query latency (milliseconds per query) on **Uniform** data within a bounding box of $\Delta = 2^{16}$ for increasing input size n . Queries are generated using a **Uniform** distribution and query size $\rho = 0.01$.

n	Boost-L	Boost-Q	Boost-R*	CGAL-Kd	CGAL-R	Curve-H	Curve-Z
$5 \cdot 10^5$	2.1541	1.5572	0.7808	0.9454	7.5449	1.6084	1.5709
$10 \cdot 10^5$	3.2667	2.3674	1.1859	1.6610	11.7887	2.1430	2.1423
$50 \cdot 10^5$	10.6512	9.8765	4.0511	16.6743	37.3152	4.7086	4.7305
$100 \cdot 10^5$	23.9363	25.0254	11.4872	37.4281	67.8486	7.7133	7.7619
$200 \cdot 10^5$	57.4231	72.3076	32.3476	84.7407	-	13.6468	13.4491
$400 \cdot 10^5$	112.5997	147.2015	63.6683	183.1908	-	25.3082	23.8530

Table D.34: Query latency (milliseconds per query) on **Gaussian** data within a bounding box of $\Delta = 2^{16}$ for increasing input size n . Queries are generated using a **Uniform** distribution and query size $\rho = 0.01$.

n	Boost-L	Boost-Q	Boost-R*	CGAL-Kd	CGAL-R	Curve-H	Curve-Z
$5 \cdot 10^5$	3.6256	1.7773	0.6881	1.1582	10.1275	1.9058	1.8440
$10 \cdot 10^5$	5.4094	2.6251	0.9424	4.0432	18.6411	2.5269	2.5080
$50 \cdot 10^5$	20.3658	16.1046	6.9548	20.9744	47.8240	5.1474	5.1722
$100 \cdot 10^5$	30.0540	26.6239	10.2336	37.5189	69.3496	8.2383	8.2858
$200 \cdot 10^5$	58.2910	61.4742	25.4557	78.6343	-	14.4802	14.4450
$400 \cdot 10^5$	122.1235	169.0171	59.7940	167.1427	-	26.3340	26.0743

Table D.35: Query latency (milliseconds per query) on **Skewed** data within a bounding box of $\Delta = 2^{16}$ for increasing input size n . Queries are generated using a **Uniform** distribution and query size $\rho = 0.01$.

n	Boost-L	Boost-Q	Boost-R*	CGAL-Kd	CGAL-R	Curve-H	Curve-Z
$5 \cdot 10^5$	1.3431	1.2137	0.7786	1.1146	10.9804	1.6766	1.6523
$10 \cdot 10^5$	2.1457	1.9055	1.2014	1.8372	16.8425	2.2249	2.2343
$50 \cdot 10^5$	8.7449	7.9544	3.9286	14.9769	48.0524	5.0254	5.0622
$100 \cdot 10^5$	28.6446	33.6698	16.1353	30.3406	74.3633	8.2638	8.3830
$200 \cdot 10^5$	47.8868	52.0248	31.6547	54.9617	-	15.5075	15.3414
$400 \cdot 10^5$	105.0806	150.7486	63.2403	107.0069	-	27.5968	27.5708

Table D.36: Query latency (milliseconds per query) on **Clustered** data within a bounding box of $\Delta = 2^{16}$ for increasing input size n . Queries are generated using a **Uniform** distribution and query size $\rho = 0.01$.

n	Boost-L	Boost-Q	Boost-R*	CGAL-Kd	CGAL-R	Curve-H	Curve-Z
$5 \cdot 10^5$	4.2256	1.7575	0.7819	1.2473	8.6554	2.0226	1.9808
$10 \cdot 10^5$	6.3466	3.0186	1.1682	2.1772	13.7559	2.7214	2.7238
$50 \cdot 10^5$	19.0600	10.3285	3.5821	11.1820	45.5373	5.5216	5.6702
$100 \cdot 10^5$	30.6283	19.9684	9.4854	29.7996	66.0934	8.8593	9.0287
$200 \cdot 10^5$	50.8735	42.6690	14.6789	71.6959	-	14.9090	15.1208
$400 \cdot 10^5$	105.9867	105.6908	55.5892	177.6789	-	25.5321	26.4645

Table D.37: Query latency (milliseconds per query) on **Uniform** data within a bounding box of $\Delta = 2^{16}$ for increasing input size n . Queries are generated using a **Gaussian** distribution and query size $\rho = 0.01$.

n	Boost-L	Boost-Q	Boost-R*	CGAL-Kd	CGAL-R	Curve-H	Curve-Z
$5 \cdot 10^5$	7.0961	5.6472	2.6022	3.1123	19.6766	4.0434	4.1305
$10 \cdot 10^5$	11.1551	8.8399	4.1814	5.9413	33.4441	6.0500	6.2933
$50 \cdot 10^5$	38.5951	38.4871	15.8550	71.6025	136.9613	17.6475	17.6732
$100 \cdot 10^5$	94.6226	102.7044	45.1396	168.8020	247.7664	31.7142	31.4030
$200 \cdot 10^5$	213.7405	311.2647	151.8829	402.3335	-	59.1649	58.0067
$400 \cdot 10^5$	504.2864	642.8760	303.2738	818.4914	-	114.0356	110.3563

Table D.38: Query latency (milliseconds per query) on **Gaussian** data within a bounding box of $\Delta = 2^{16}$ for increasing input size n . Queries are generated using a **Gaussian** distribution and query size $\rho = 0.01$.

n	Boost-L	Boost-Q	Boost-R*	CGAL-Kd	CGAL-R	Curve-H	Curve-Z
$5 \cdot 10^5$	2.8349	1.6510	0.4880	0.8609	5.8051	1.5339	1.4796
$10 \cdot 10^5$	4.0729	2.4141	0.6648	1.4751	13.3485	2.0052	1.9449
$50 \cdot 10^5$	9.6849	9.5318	2.0234	8.7106	31.4847	3.6344	3.5969
$100 \cdot 10^5$	15.3948	18.6199	3.4934	12.9000	47.5541	5.4141	5.5293
$200 \cdot 10^5$	24.1815	38.6224	6.6800	43.9816	-	8.6790	8.8100
$400 \cdot 10^5$	59.8516	117.8170	24.1298	89.5295	-	14.6103	14.7328

Table D.39: Query latency (milliseconds per query) on **Skewed** data within a bounding box of $\Delta = 2^{16}$ for increasing input size n . Queries are generated using a **Gaussian** distribution and query size $\rho = 0.01$.

n	Boost-L	Boost-Q	Boost-R*	CGAL-Kd	CGAL-R	Curve-H	Curve-Z
$5 \cdot 10^5$	1.2577	1.0707	0.7035	1.0439	7.9387	1.4190	1.5128
$10 \cdot 10^5$	1.9679	1.9101	1.0681	1.6067	15.9834	2.0463	2.1280
$50 \cdot 10^5$	7.2726	6.7214	3.3141	6.1738	42.1406	4.6897	4.7162
$100 \cdot 10^5$	18.4878	23.0518	8.9346	26.3706	70.4151	8.2148	8.3921
$200 \cdot 10^5$	30.0219	32.0450	16.6992	45.7239	-	14.9863	15.1276
$400 \cdot 10^5$	87.6271	123.7484	54.5533	96.9876	-	26.3186	26.1563

Table D.40: Query latency (milliseconds per query) on **Clustered** data within a bounding box of $\Delta = 2^{16}$ for increasing input size n . Queries are generated using a **Gaussian** distribution and query size $\rho = 0.01$.

n	Boost-L	Boost-Q	Boost-R*	CGAL-Kd	CGAL-R	Curve-H	Curve-Z
$5 \cdot 10^5$	3.4373	1.5617	0.7682	1.2640	10.3466	2.0408	2.0247
$10 \cdot 10^5$	5.4301	2.5131	1.1567	2.1932	15.7971	2.7162	2.7688
$50 \cdot 10^5$	16.9494	8.8049	3.6662	15.6427	42.5222	5.5168	5.7097
$100 \cdot 10^5$	30.8110	27.5617	7.8600	36.0106	74.1120	8.7989	9.0472
$200 \cdot 10^5$	59.0912	47.5525	20.3554	77.3335	-	14.9991	15.1940
$400 \cdot 10^5$	121.6091	113.7955	49.6833	182.3177	-	27.0570	26.8465

Table D.41: Query latency (milliseconds per query) on **Uniform** data within a bounding box of $\Delta = 2^{16}$ for increasing input size n . Queries are generated using a **Skewed** distribution and query size $\rho = 0.01$.

n	Boost-L	Boost-Q	Boost-R*	CGAL-Kd	CGAL-R	Curve-H	Curve-Z
$5 \cdot 10^5$	1.2941	0.8894	0.4769	0.5815	4.9066	1.1287	1.1587
$10 \cdot 10^5$	2.0557	1.3612	0.7145	1.0063	7.8684	1.4588	1.5234
$50 \cdot 10^5$	6.2034	5.3671	2.3015	8.3460	23.7074	2.8347	2.9206
$100 \cdot 10^5$	15.7719	17.0422	7.9343	21.8482	43.0711	4.4799	4.5718
$200 \cdot 10^5$	29.5636	37.7868	16.2935	45.4971	-	7.6113	7.6546
$400 \cdot 10^5$	57.3901	75.7232	32.3427	88.9624	-	13.7659	13.5528

Table D.42: Query latency (milliseconds per query) on **Gaussian** data within a bounding box of $\Delta = 2^{16}$ for increasing input size n . Queries are generated using a **Skewed** distribution and query size $\rho = 0.01$.

n	Boost-L	Boost-Q	Boost-R*	CGAL-Kd	CGAL-R	Curve-H	Curve-Z
$5 \cdot 10^5$	5.3863	2.5947	1.0595	2.1499	17.3942	2.8912	2.9492
$10 \cdot 10^5$	8.3500	4.2814	1.7105	7.9441	27.3805	4.0618	4.1732
$50 \cdot 10^5$	39.6281	30.4510	14.1913	45.9586	80.6998	10.0033	10.2356
$100 \cdot 10^5$	58.5960	68.0041	21.0257	84.6633	138.4158	17.2095	17.3390
$200 \cdot 10^5$	120.1825	121.7272	69.8919	185.4262	-	31.4824	31.0219
$400 \cdot 10^5$	267.4562	331.8026	143.4502	381.9929	-	59.0552	58.0548

Table D.43: Query latency (milliseconds per query) on **Skewed** data within a bounding box of $\Delta = 2^{16}$ for increasing input size n . Queries are generated using a **Skewed** distribution and query size $\rho = 0.01$.

n	Boost-L	Boost-Q	Boost-R*	CGAL-Kd	CGAL-R	Curve-H	Curve-Z
$5 \cdot 10^5$	1.2736	1.1025	0.7377	1.0777	9.7734	1.5442	1.5701
$10 \cdot 10^5$	1.8860	1.8668	1.1689	1.7466	18.0484	2.0860	2.2074
$50 \cdot 10^5$	8.4397	7.6730	3.5891	10.3217	46.7672	5.1121	5.2260
$100 \cdot 10^5$	15.5803	19.4369	7.2569	23.9422	71.6563	8.0498	8.2498
$200 \cdot 10^5$	36.8461	39.9797	18.6518	50.7521	-	14.2765	14.5056
$400 \cdot 10^5$	99.1955	131.4727	59.0577	104.6831	-	26.2734	26.2893

Table D.44: Query latency (milliseconds per query) on **Clustered** data within a bounding box of $\Delta = 2^{16}$ for increasing input size n . Queries are generated using a **Skewed** distribution and query size $\rho = 0.01$.

n	Boost-L	Boost-Q	Boost-R*	CGAL-Kd	CGAL-R	Curve-H	Curve-Z
$5 \cdot 10^5$	1.7103	0.7418	0.4090	0.8153	3.3602	1.2922	1.3122
$10 \cdot 10^5$	2.9522	1.3245	0.6629	1.4878	4.8519	1.8454	1.9413
$50 \cdot 10^5$	10.7941	5.2450	2.1947	5.9645	11.7107	4.5273	4.7395
$100 \cdot 10^5$	18.0006	10.5543	3.8249	11.9503	24.6181	7.6655	7.9512
$200 \cdot 10^5$	30.3592	24.3907	7.3290	24.7131	-	13.4933	13.7353
$400 \cdot 10^5$	60.3249	53.1593	14.3698	57.3812	-	24.4621	24.5457

Table D.45: Query latency (milliseconds per query) on **Uniform** data within a bounding box of $\Delta = 2^{16}$ for increasing input size n . Queries are generated using a **Clustered** distribution and query size $\rho = 0.01$.

n	Boost-L	Boost-Q	Boost-R*	CGAL-Kd	CGAL-R	Curve-H	Curve-Z
$5 \cdot 10^5$	1.1467	0.8239	0.4743	0.6635	2.0173	1.0903	1.0971
$10 \cdot 10^5$	1.6981	1.4363	0.7542	1.2437	2.8296	1.5856	1.6157
$50 \cdot 10^5$	6.9790	6.9101	2.8859	5.8647	8.8317	4.1571	4.1918
$100 \cdot 10^5$	11.7240	13.1559	4.4818	14.1133	24.4644	7.4341	7.4813
$200 \cdot 10^5$	21.4278	27.9088	8.8910	31.2907	-	13.3767	13.1153
$400 \cdot 10^5$	25.0396	42.1989	18.1149	63.0104	-	18.0760	21.5553

Table D.46: Query latency (milliseconds per query) on **Gaussian** data within a bounding box of $\Delta = 2^{16}$ for increasing input size n . Queries are generated using a **Clustered** distribution and query size $\rho = 0.01$.

n	Boost-L	Boost-Q	Boost-R*	CGAL-Kd	CGAL-R	Curve-H	Curve-Z
$5 \cdot 10^5$	1.2610	0.7000	0.3118	0.6115	2.7223	1.0682	1.0187
$10 \cdot 10^5$	2.0115	1.0906	0.4927	1.0819	3.8613	1.4724	1.4529
$50 \cdot 10^5$	6.4502	4.8311	1.7152	4.8173	10.8953	4.1079	4.1799
$100 \cdot 10^5$	12.0065	11.0399	3.5859	10.1039	21.5195	6.6851	6.7993
$200 \cdot 10^5$	19.8914	22.5584	6.6525	21.6654	-	11.0544	11.1275
$400 \cdot 10^5$	28.5594	42.6896	11.5503	47.7311	-	17.1260	17.0543

Table D.47: Query latency (milliseconds per query) on **Skewed** data within a bounding box of $\Delta = 2^{16}$ for increasing input size n . Queries are generated using a **Clustered** distribution and query size $\rho = 0.01$.

n	Boost-L	Boost-Q	Boost-R*	CGAL-Kd	CGAL-R	Curve-H	Curve-Z
$5 \cdot 10^5$	0.6042	0.5342	0.3922	0.6574	2.8906	1.0543	1.0784
$10 \cdot 10^5$	1.0268	0.9235	0.6458	1.1243	4.3701	1.4003	1.4432
$50 \cdot 10^5$	4.4714	3.9671	2.0905	4.2559	12.2627	4.1979	4.2314
$100 \cdot 10^5$	8.8141	9.6912	3.9539	7.5223	16.7468	7.0504	7.2450
$200 \cdot 10^5$	15.1206	17.7678	7.1159	13.8934	-	13.1730	13.2044
$400 \cdot 10^5$	26.4786	40.5410	12.6118	23.1486	-	23.3158	23.1843

Table D.48: Query latency (milliseconds per query) on **Clustered** data within a bounding box of $\Delta = 2^{16}$ for increasing input size n . Queries are generated using a **Clustered** distribution and query size $\rho = 0.01$.

D.5 Raw data for the parallel experiments

Construction time of the data structures using parallel computation on synthetic data sets for increasing n .

n	Boost-L	Boost-Q	Boost-R*	CGAL-Kd	CGAL-R	Curve-H	Curve-Z
$5 \cdot 10^5$	0.0437	0.0432	0.0434	0.0023	1.2561	0.0413	0.0218
$10 \cdot 10^5$	0.0928	0.0922	0.0926	0.0044	2.8403	0.0884	0.0426
$50 \cdot 10^5$	0.5617	0.5653	0.5619	0.0216	17.8072	0.4316	0.1956
$100 \cdot 10^5$	1.2097	1.1865	1.1861	0.0442	38.6311	0.8748	0.3985
$200 \cdot 10^5$	2.6552	2.6515	2.6488	0.0915	-	1.7571	0.8489
$400 \cdot 10^5$	5.1020	5.0890	5.0936	0.1735	-	3.3071	1.6373

Table D.49: Construction time (in seconds) on **Uniform** data within a bounding box of $\Delta = 2^{16}$ for increasing input size n .

n	Boost-L	Boost-Q	Boost-R*	CGAL-Kd	CGAL-R	Curve-H	Curve-Z
$5 \cdot 10^5$	0.0444	0.0452	0.0442	0.0022	1.2757	0.0433	0.0205
$10 \cdot 10^5$	0.0936	0.0938	0.0929	0.0043	2.8418	0.0789	0.0429
$50 \cdot 10^5$	0.5640	0.5604	0.5557	0.0218	17.7692	0.4198	0.1939
$100 \cdot 10^5$	1.2000	1.1938	1.1913	0.0443	38.2545	0.7914	0.3999
$200 \cdot 10^5$	2.4791	2.4798	2.4753	0.0874	-	1.5912	0.8034
$400 \cdot 10^5$	5.0419	5.0367	5.0365	0.1742	-	3.4390	1.7314

Table D.50: Construction time (in seconds) on **Gaussian** data within a bounding box of $\Delta = 2^{16}$ for increasing input size n .

n	Boost-L	Boost-Q	Boost-R*	CGAL-Kd	CGAL-R	Curve-H	Curve-Z
$5 \cdot 10^5$	0.0442	0.0444	0.0441	0.0022	1.2651	0.0409	0.0207
$10 \cdot 10^5$	0.0912	0.0919	0.0923	0.0044	2.8736	0.0807	0.0405
$50 \cdot 10^5$	0.5594	0.5529	0.5568	0.0219	17.7780	0.4255	0.1951
$100 \cdot 10^5$	1.1968	1.1961	1.1926	0.0437	38.2665	0.8049	0.3970
$200 \cdot 10^5$	2.5149	2.5149	2.5081	0.0871	-	1.7278	0.8014
$400 \cdot 10^5$	5.0809	5.0812	5.0822	0.1745	-	3.4926	1.7310

Table D.51: Construction time (in seconds) on **Skewed** data within a bounding box of $\Delta = 2^{16}$ for increasing input size n .

n	Boost-L	Boost-Q	Boost-R*	CGAL-Kd	CGAL-R	Curve-H	Curve-Z
$5 \cdot 10^5$	0.0370	0.0373	0.0373	0.0022	1.1843	0.0382	0.0182
$10 \cdot 10^5$	0.0781	0.0791	0.0804	0.0043	2.7906	0.0692	0.0350
$50 \cdot 10^5$	0.4610	0.4595	0.4571	0.0221	16.0696	0.3375	0.1768
$100 \cdot 10^5$	0.9399	0.9359	0.9383	0.0443	33.8600	0.7269	0.3468
$200 \cdot 10^5$	1.9831	1.9831	1.9730	0.0880	-	1.4657	0.6954
$400 \cdot 10^5$	4.5295	4.5295	4.3323	0.1809	-	2.7606	1.4242

Table D.52: Construction time (in seconds) on **Clustered** data within a bounding box of $\Delta = 2^{16}$ for increasing input size n .